trum, however, and apparently represents a no-phonon excited electronic state of the bound exciton. It is notable that this line broadens more rapidly than X_0 and X_0' as the temperature is increased from 100 to 400°K, presumably due to a decrease in the excited-state lifetime arising from enhanced dissociation by phonon interactions. There is a low-energy threshold near 5.35 eV for the acoustical phonon optical absorption replicas, again corresponding to a phonon energy of 65 meV. The well-defined threshold near 5.35 eV in Fig. 8 does not have a counterpart in the emission spectrum of Fig. 7 and is therefore attributed to a no-phonon absorption line in Table I. The high-energy cutoff at the Raman energy above X_0 and X_0' is not as well defined in absorption as it is in luminescence probably because it is obscured by transverse optical replicas of the no-phonon line at ~5.28 eV.

D. Multiple Phonon Bands

These bands X_2 and X_3 in Fig. 1 show no fine structure, and since there are no longer any selection rules relevant to the emission of a second or third phonon this is to be expected. However, the low-energy thresholds indicate that successive Raman phonons are selected in the limiting case (Table I). The multiple phonon optical absorption replicas of the $N9$ system are distorted by overlap with the intrinsic interband absorption processes.[8]

E. Other Luminescence Features

The broad band near 5.02 eV in Fig. 1 may be due to a residual amount of damage in the crystal since a sharp line and band system ($1D$) which contributes luminescence in this region is often seen in specimens showing $N9$ luminescence and was observed extremely strongly in an artificially damaged specimen.

The connection between the $1D$ system and lattice damage will be the subject of further experiment.

IV. CONCLUSIONS

The recently proposed interpretation for the $N9$ system has been seen to be consistent with the transitions observed in luminescence. The luminescence has been attributed to the recombination of excitons bound to nitrogen-aluminium nearest-neighbor pairs. Phonon replicas have been identified by a comparison of the $N9$ absorption and emission spectra. Some of the phonon energies thereby deduced are consistent with those known to be selected in indirect interband transitions. The effects of the relatively large exciton binding energy in the $N9$ center compared with an exciton complex involving aluminium acceptor centers are shown to be qualitatively similar to those observed in other Group IV crystals.

ACKNOWLEDGMENTS

We would like to thank W. F. Cotty (Industrial Distributors, London) and Dr. F. A. Raal (Diamond Research Laboratory, Johannesburg) for providing many of the specimens used in this work. We are also grateful to Dr. J. C. Male for permitting the publication of Fig. 8. One of us (D.R.W.) is indebted to the Science Research Council for the provision of a maintenance grant.

PHYSICAL REVIEW VOLUME 154, NUMBER 3 15 FEBRUARY 1967

Electroreflectance at a Semiconductor-Electrolyte Interface*

MANUEL CARDONA, KERRY L. SHAKLEE, AND FRED H. POLLAK
Physics Department, Brown University, Providence, Rhode Island
(Received 28 July 1966)

The electroreflectance spectra of Si, Ge, α-Sn, AlSb, GaP, GaAs, GaSb, InP, InAs, InSb, ZnO, ZnTe, CdS, CdSe, and CdTe are reported. The measurements were performed by the electrolyte technique in the 1- to 6-eV photon energy range. The data were processed by the Kramers-Kronig technique and the variation in ϵ_1 and ϵ_2 induced by the applied electric field obtained. Several sharp peaks were observed in all these spectra and interpreted in terms of critical points in the joint density of states for optical transitions. As a result, a large number of direct interband energy gaps and spin-orbit splittings is obtained. These spin-orbit splittings are interpreted and correlated by using the $\mathbf{k}\cdot\mathbf{p}$ method: Enough experimental information is available to determine the effects of spin-orbit interaction on the valence bands of most of these materials at any point in $\mathbf{k}$ space.

I. INTRODUCTION

MODULATION techniques have been employed recently in optical reflection and absorption measurements of solids to achieve greater sensitivity and resolution. All these techniques have, as a common feature, the application of a small perturbation such as a change in lattice constant or an external field which destroys some invariant property of the crystal structure. The perturbation is made sinusoidally dependent on time, and thus a sinusoidal modulation of the response of the sample material to optical excitation is

* Supported by the National Science Foundation and the U. S. Army Research Office, Durham.

obtained. It is possible then, using conventional phase-sentitive detection techniques, to extract this small change from large and broad reflection or absorption backgrounds. The result is a derivative-like output which exhibits sharp structure in the neighborhood of direct interband edges.

The modulation techniques which have been successful to date are electroabsorption,[1–3] electroreflectance,[4,5] piezoreflectance,[6] and piezoabsorption.[7] Electroreflectance experiments have been performed in semiconductors and semimetals[4,5] by allowing the electric field to penetrate in a lossless way a distance from the surface (screening length) of the order of the penetration depth of the light. Measurements can also be performed by using the large electric fields obtained at a *p-n* junction.[2] In insulators, uniform fields can be obtained by "brute force," placing the sample between condenser plates.[1,3] The electroreflectance technique, however, does not seem quite as fruitful for metals because of their small screening lengths. Recent electroreflectance data for metals[8] reproduce structure in their optical constants, apparently because of a modulation in the refractive index of the medium in contact with the metal (water) by the electric field. Such measurements do not yield sharp structure since it is not the derivative of the optical constants of the metal with respect to the modulating parameter which is obtained.

Piezoreflectance[6] and piezoabsorption[7] techniques are applicable to metals, semiconductors, and insulators, but the spectra obtained do not seem to be as sharp as those obtained by electroreflectance or electroabsorption for semiconductors. Piezoreflectance experiments are also difficult to perform because of the large spurious signals produced by mechanical vibrations.

This paper reports the room-temperature electroreflectance spectra[4] of several materials with the germanium structure (Si, Ge, α-Sn), the zinc-blende structure (AlSb, GaP, GaAs, GaSb, InP, InAs, InSb, HgTe, HgSe, ZnTe, CdTe, CdS) and the wurtzite structure (CdS, CdSe, ZnO), as measured by the electrolyte technique.[5] These spectra are transformed into changes in the real and imaginary parts of the dielectric constant (ϵ_1 and ϵ_2 respectively) by means of a Kramers-Kronig analysis. This information is interpreted and discussed in terms of the existing theory of electroreflectance and the available knowledge of the band structures of these semiconductors.

[1] M. Chester and P. H. Wendland, Phys. Rev. Letters **13**, 193 (1964).
[2] A. Frova, P. Handler, F. A. Germano, and D. E. Aspnes, Phys. Rev. **145**, 575 (1966).
[3] Y. Yacoby, Phys. Rev. **142**, 445 (1965).
[4] B. O. Seraphin and R. B. Hess, Phys. Rev. Letters **14**, 138 (1965).
[5] K. L. Shaklee, F. H. Pollak, and M. Cardona, Phys. Rev. Letters **15**, 883 (1965).
[6] W. E. Engeler, H. Fritzsche, M. Garfinkel, and J. J. Tiemann, Phys. Rev. Letters **14**, 1069 (1965); G. O. Gobeli and E. O. Kane, *ibid.* **15**, 142 (1965).
[7] W. E. Engeler, M. Garfinkel, and J. J. Tiemann, Phys. Rev. Letters **16**, 239 (1966).
[8] J. Feinleib, Phys. Rev. Letters **16**, 1200 (1966).

At present electroreflectance provides the best sensitivity and resolution of the several optical techniques available for optical measurements on semiconductors above the fundamental absorption edge. In particular, the resolution and sensitivity are much better than those obtained by conventional reflectivity measurements, which provide most of the existing information about semiconductors above the fundamental absorption edge. Electroreflectance provides the accuracy and sensitivity needed to study the variation of interband energy gaps with various static parameters such as temperature, uniaxial stress,[9] and doping (e.g. the Burstein shift). We present in Sec. II a brief review of what is known about the optical properties and band structures of semiconductors since this information will be used to interpret electroreflectance spectra in later sections. The present state of the theory of electroreflectance (Franz-Keldysh effect) is given in Sec. III. In Sec. IV the experimental technique used for our electroreflectance measurements is described. The results obtained are presented in Sec. V. The results of the Kramers-Kronig analysis of the electroreflectance spectra of a few materials are presented in Sec. VI. Section VII contains a discussion of the results, with emphasis on the new information about band structures, spin-orbit splittings, and the electro-optic effect that has been gained from our measurements.

II. OPTICAL PROPERTIES AND ENERGY BAND STRUCTURE

The crystal structures of wurtzite-, zinc-blende-, and germanium-type materials are very similar and therefore great similarities also exist between their optical properties and energy band structures. Hence it is convenient to discuss in detail a representative material of this family and then point out the specific differences between the three families. Germanium is the ideal material for this purpose. It is centrally located in the family; its electronic optical properties have been thoroughly studied,[10] and accurate semiempirical band-structure calculations are available.[11,12]

Germanium

The normal-incidence reflection spectrum of germanium is shown in Fig. 1 together with the absorption spectrum in the neighborhood of the fundamental edge (at room temperature). The peaks in the spectrum are attributed to direct interband transitions (see Fig. 2) at points in **k** space at which the combined density of states for optical transitions has a singularity.

[9] F. H. Pollak, M. Cardona, and K. L. Shaklee, Phys. Rev. Letters **16**, 942 (1966).
[10] See, for instance, J. C. Phillips, in *Solid State Physics*, edited by F. Seitz and D. Turnbull (Academic Press Inc., New York, 1966), and M. Cardona, in *Proceeding of the 7th International Conference on the Physics of Semiconductors, Paris, 1964* (Dunod Cie, Paris, 1964).
[11] D. Brust, Phys. Rev. **134**, A1337 (1964).
[12] M. Cardona and F. H. Pollak, Phys. Rev. **142**, 530 (1966).

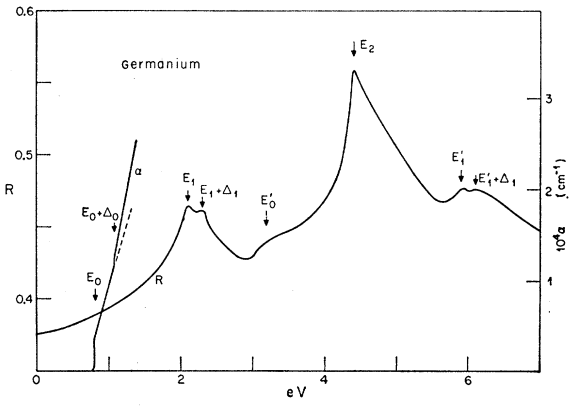

FIG. 1. Normal-incidence reflection spectrum of germanium (from Ref. 45) and absorption spectrum near the direct edge E_0 [from M. V. Hobden, J. Phys. Chem. Solids **23**, 821 (1962)].

The combined density of states has singularities[10] whenever

$$\nabla_{\mathbf{k}}(E_c-E_v)=0, \tag{1}$$

where E_c and E_v are the energies of the conduction and valence bands respectively. These transitions occur at a photon energy $\hbar\omega=E_c-E_v$. Equation (1) is satisfied at high symmetry points (Γ, X, L in germanium and zincblende), where $\nabla_{\mathbf{k}}E_c=\nabla_{\mathbf{k}}E_v=0$. One should observe structure due to transitions at these points provided the matrix element is not zero on account of a group-theoretical selection rule. It is also possible for $\nabla_{\mathbf{k}}(E_c-E_v)$ to be accidentally zero along high symmetry lines such as [111] (see Fig. 2) without $\nabla_{\mathbf{k}}E_c$ being zero. Four types of critical points for which Eq. (1) is satisfied are possible depending[11] on the signs of the quadratic terms in the expansion of E_c-E_v as a function of $\mathbf{k}$:

$$E_c-E_v=\frac{\hbar^2}{2m}\left[\frac{k_x^2}{m_x}+\frac{k_y^2}{m_y}+\frac{k_z^2}{m_z}\right]+E_g. \tag{2}$$

If all effective masses are positive the critical point is a minimum (M_0). If only one (M_2) or two (M_1) masses are positive, one has a saddle point. A maximum (M_3) corresponds to all masses in Eq. (2) negative.

The lowest energy structure shown in Fig. 1 (E_0 at 0.80 eV) corresponds to the direct absorption edge at $\mathbf{k}=0$ (see Fig. 2). It is seen only in transmission and its counterpart on the reflection spectrum has not been resolved. This is due to the small density of states associated with these transitions: they occur at $\mathbf{k}=0$ and the effective mass of the $\Gamma_{2'}$ conduction band is very small as a result of the small $\Gamma_{25'}-\Gamma_{2'}$ gap. The E_0 transitions can be seen in the reflection spectrum of higher band gap materials (e.g., GaP[13] and most II–IV compounds[14–16]). The $E_0+\Delta_0$ transitions are seen, for the same reasons, only in the absorption spectrum of Fig. 1. They begin at 1.09 eV and correspond to transitions at $\mathbf{k}=0$ between the lower $\Gamma_{25'}$ valence band (Γ_7^+), split from Γ_8^+ by spin-orbit interaction. The spin-orbit splittings Δ_0 of the $\Gamma_{25'}$ state found by this method agree well with those obtained from transitions between the various valence bands in p-type materials.[17]

Above the fundamental edge there is a second set of peaks labeled E_1 and $E_1+\Delta_1$. Since the splitting of these peaks ($\Delta_1\simeq 0.2$ eV) is about two-thirds of the spin-orbit splitting at $\Gamma_{25'}$, it is believed that the transitions responsible for them occur mainly in the [111] direction. The Δ_1 splitting is then produced by the action of the spin-orbit interaction on the Λ_3 orbital doublet. Density-of-states calculations by the pseudopotential method[11] place the corresponding critical point at $k=(\pi/a)(0.3, 0.3, 0.3)$. Symmetry predicts another critical point in the [111] direction at the edge of the zone ($L_{3'}-L_1$). Weak structure due to this critical point and the $L_{3'}$ spin-orbit splitting has been observed by Potter[18] slightly below the E_1, $E_1+\Delta_1$ peaks.

The next structure in the reflection spectrum E_0' has been assigned[10] to transitions at or near $\mathbf{k}=0$ between the $\Gamma_{25'}$ and the Γ_{15} bands. Some fine structure due to spin-orbit splittings of $\Gamma_{25'}$ and Γ_{15} is expected but not resolved in Fig. 1. Actually, the nearly parallel nature of the Δ_5 and Δ_1 bands in the [100] direction (see Fig. 2) indicates the possibility[11] of having more than one critical point near $\mathbf{k}=0$. The position of these critical points is affected very drastically by spin-orbit interaction and hence a detailed assignment of the E_0' transitions has to await density of states calculations with the inclusion of spin-orbit splitting.

The next structure E_2 at 4.45 eV, the strongest peak of the spectrum, has been attributed[10] to an accidental coincidence of an M_1 saddle point at $X(X_4\rightarrow X_1)$ and

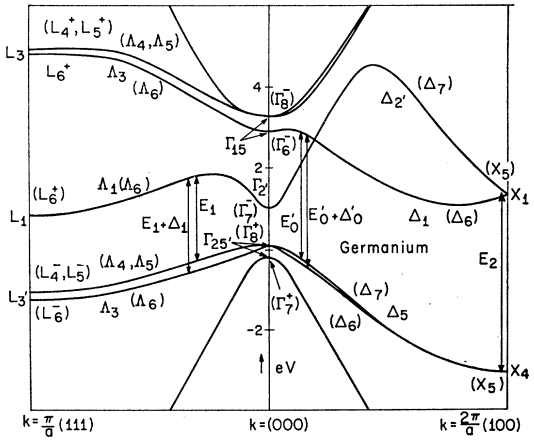

FIG. 2. Band structure of germanium obtained by the $\mathbf{k}\cdot\mathbf{p}$ method (see Ref. 12).

[13] R. Zallen and W. Paul, Phys. Rev. **134**, A1628 (1964).
[14] M. Cardona, J. Appl. Phys. **32S**, 958 (1961).
[15] M. Cardona and D. L. Greenaway, Phys. Rev. **131**, 98 (1963).
[16] D. Dutton, Phys. Rev. **112**, 785 (1958).
[17] R. Braunstein and E. O. Kane, J. Phys. Chem. Solids **23**, 1423 (1962).
[18] R. F. Potter, Phys. Rev. **150**, 562 (1966).

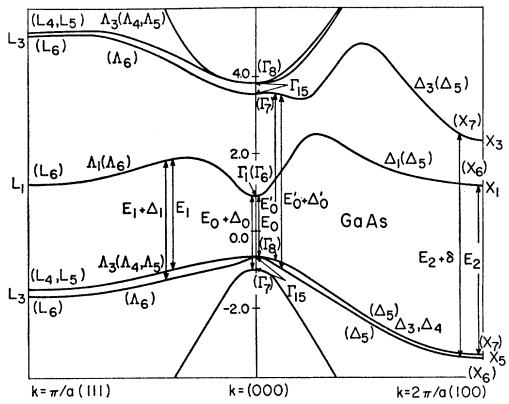

FIG. 3. Band structure of GaAs obtained by the $\mathbf{k}\cdot\mathbf{p}$ method (see Ref. 81).

an M_2 saddle point in the [110] direction ($\Sigma_3 \rightarrow \Sigma_2$).[19] This assignment has become questionable recently as a result of band calculations for silicon by Kane.[20] The main contribution to the E_2 peak seems to come indeed from Σ transitions but not from X transitions ($X_4 \rightarrow X_1$ transitions actually do not take place at a critical point since the X_1 slopes are finite). Instead, for silicon, (no calculations are available for germanium) a large region of $\mathbf{k}$ space around the point $(2\pi/a)(\frac{3}{8},\frac{3}{8},\frac{3}{4})$ seems to give a large contribution to the E_2 peak.

The E_1' structure of Fig. 1 is believed[10] due to $L_{3'} \rightarrow L_3$ transitions. The splitting, also 0.2 eV, corresponds to the $L_{3'}$ spin-orbit splitting: the L_3 spin-orbit splitting is considerably smaller[12] than that of $L_{3'}$.

Qualitative differences between the optical spectra of group IV materials stem mainly from the relative position of $\Gamma_{2'}$ with respect to the $\Gamma_{25'}$ and Γ_{15} states. $\Gamma_{2'}$ is s like and hence depends drastically on the element under consideration. In diamond and silicon $\Gamma_{2'}$ is above Γ_{15} and hence the smallest direct edge is not $E_0(\Gamma_{25'} \rightarrow \Gamma_{2'})$ but $E_0'(\Gamma_{25'} \rightarrow \Gamma_{15})$. In gray tin the ordering of the orbital levels is the same as in germanium but the $\Gamma_{25'}-\Gamma_{2'}$ gap is very small: the large spin-orbit interaction brings the Γ_8^+ component of $\Gamma_{25'}$ above $\Gamma_{2'}$ and the material becomes a semimetal.[21]

The zinc-blende-type materials differ from germanium by the absence of inversion symmetry.[22] The lowered symmetry produces the splitting of the orbital degeneracy at X_1 into X_1 and X_3 (see Figs. 2 and 3). A splitting of the E_2 peak, probably associated with the X_1 and X_3 splitting, has been reported for a number of III–V and II–VI compounds.[10] The X_4-X_1 gap of germanium becomes $X_5 \rightarrow (X_1,X_3)$ in zincblende and produces two critical points: $X_5 \rightarrow X_1$, $X_5 \rightarrow X_3$. The corresponding two peaks in the optical spectra have been labelled E_2 and $E_2+\delta$. A similar orbital splitting occurs along the X-W line (diagonal of the square faces of the Brillouin zone) while the crossing of the Δ_1 and $\Delta_{2'}$ bands of germanium in the [100] direction is removed: both bands have the same zinc-blende symmetry (Δ_1). The addition of spin-orbit interaction does not split the double (quadruple with spin) degeneracy of the X_4 state in germanium. This is not the case in zincblende: The X_5 state splits into two states (doubly degenerate) X_6 and X_7 when spin-orbit effects are included. Evidence of this splitting has been reported for several II-VI materials.[10] The space-time reversal degeneracy (sometimes referred to as Kramers degeneracy) of germanium is lifted in zincblende. As a result the spin degeneracy splits in all but the high symmetry [111] and [100] directions.[23] This splitting is small in III–V compounds and no observations relating to it have been reported. An even smaller splitting of the spin degeneracy of the Γ_{15} bands in the [111] and [100] directions[24] has not been experimentally observed either.

Wurtzite has a hexagonal crystal structure which can be thought of as composed of two interpenetrating hexagonal close-packed lattices of the two constituent atoms. The environment of each atom is tetrahedral and hence the nearest neighbor structure is very similar to that of zincblende.[25] Most of the II–VI compounds can be obtained in both zinc-blende and wurtzite structures although, with the exception of ZnS, large single crystals can only be obtained in one of the two structures.

A relationship between the band structures of zincblende and wurtzite can be easily obtained by using the tight-binding approximation.[25] The volume of the hexagonal Brillouin zone of wurtzite is half that of zincblende due to the doubling in the number of atoms per unit cell. The [111] direction of zincblende is made to correspond to the [001] direction of wurtzite (hexagonal axis) but the L point is folded onto $\mathbf{k}=0$ so as to half the size of the Brillouin zone. The states along the c axis of wurtzite can then be obtained by applying a small hexagonal perturbation to the [111] states of zincblende. The top of the valence band Γ_8 splits into Γ_7 and Γ_9 under the action of the hexagonal field but the splitting is quite small ($\sim$0.02 eV as found experimentally). This splitting is responsible for the polarization effects observed at the fundamental edge of wurtzite. A correspondence between other zinc-blende and wurtzite directions cannot be rigorously established. Intuitively, however, it is clear that the [111], [$\bar{1}$11],

[19] These states have often been labeled Σ_4 and Σ_1. According to Koster's notation they are, however, Σ_3 and Σ_2.

[20] E. O. Kane, Phys. Rev. **146**, 558 (1966).

[21] S. Groves and W. Paul, Phys. Rev. Letters **11**, 194 (1963).

[22] Strictly speaking germanium does not have inversion symmetry. The inversion as a symmetry operation must always be accompanied by a translation ($a/4$, $a/4$, $a/4$). The groups of the $\mathbf{k}$ vector are, however, isomorphic to the groups obtained eliminating the translation except for points on the X-W line (diagonal of the square faces of the Brillouin zone). See, for instance, G. Koster, in *Solid State Physics*, edited by F. Seitz and D. Turnbull (Academic Press Inc., New York, 1957).

[23] M. Cardona, F. H. Pollak, and J. G. Broerman, Phys. Letters **19**, 276 (1965).

[24] G. Dresselhaus, Phys. Rev. **100**, 580 (1955).

[25] J. Birman, Phys. Rev. **115**, 1493 (1959).

$[1\bar{1}1]$, $[11\bar{1}]$ degeneracy is going to be split in wurtzite. The $[\bar{1}11]$ $[1\bar{1}1]$ $[11\bar{1}]$ critical points of zincblende will probably shift to lower symmetry points of the wurtzite zone and the E_1 structure of zincblende will be split in wurtzite. The [111] E_1 transitions are only allowed for the electric field $\mathbf{E}$ perpendicular to [111]. Hence strong polarization effects should appear in the E_1 structure of wurtzite[26]: two peaks, both with spin-orbit splittings, are seen for $\mathbf{E}\perp c$ and only one for $\mathbf{E}\|c$. Structure similar to E_2 is also observed in wurtzite but will not be discussed here since it lies beyond the present energy range of the electroreflectance technique.

III. ELECTROREFLECTANCE THEORY

It is generally accepted that the gross features of the electroreflectance spectra are related to the Franz-Keldysh effect.[27–31] Effects of the quantization by the electric field of the electron orbits in $\mathbf{k}$ space (the so-called Stark effect[29]) have not been observed. The spacing in energy of the Stark ladder ($\Delta E=ea|\mathbf{F}|$, a=lattice constant, $\mathbf{F}$=electric field) is very small for the fields obtained in practice and the non-uniform nature of the fields at space-charge barriers probably smears out the Stark levels.

The presence of the uniform electric field destroys the translational symmetry of the crystal. For a small applied electric field it is conventional to picture the crystal as having a local band structure around a given crystal point, with the origin of energy varying linearly with distance along the direction of the electric field. Under these conditions, the energy gap disappears: the top of the valence band at a given crystal point is always degenerate with the bottom of the conduction band at another crystal point because of the energy of the external electric field. Optical transitions become possible below the energy gap but, because of the decreasing overlap of the valence- and conduction-band wave functions, the absorption coefficient decays exponentially with $\hbar\omega-E_g$. This gives rise to an apparent decrease of the energy gap with electric field in transmission experiments with moderately thick samples. This effect—usually called the Franz-Keldysh effect—can be treated in the effective-mass approximation. In this approximation the Stark levels are automatically removed. The imaginary part of the dielectric constant ϵ_2 is given by[30–32]:

$$\epsilon_2=\frac{4\pi^2e^2}{m^2\omega^2}\sum|M|^2|\phi(0)|^2\delta(E_c-E_v-\hbar\omega) \qquad (3)$$

where M is the optical matrix element in the absence of the electric field $\mathbf{F}$, and $\phi(\mathbf{r})$ is the wave function of the relative coordinates of the electron-hole pair in the presence of the electric field as obtained by solving the appropriate effective-mass equation. The real part of the dielectric constant ϵ_1 can be readily obtained by applying to ϵ_2 the Kramers-Kronig transform.

The effective mass equation must include, in principle, beside the uniform electric field the Coulomb interaction between the electron and hole (exciton effects). Since inclusion of this term makes the three-dimensional effective mass equation nonseparable, it is normally assumed that the external field is much larger than the Coulomb field and exciton effects are neglected. A discussion of exciton effects for spherical energy surfaces has been given by Duke.[33] Once exciton effects are neglected, the effective mass equation for $\phi(\mathbf{r})$ can be separated into its three components. The solution is[31]:

$$\phi(\mathbf{r})=D\,\mathrm{Ai}(-\zeta_x)\,\mathrm{Ai}(-\zeta_y)\,\mathrm{Ai}(-\zeta_z) \qquad (4)$$

where D is a normalization constant, Ai is the Airy function and

$$\zeta_i=\frac{E_i}{\hbar\psi_i}+r_i\hbar^{-2/3}(2m_i^*eF_i)^{1/3}$$

with (5)

$$\psi_i^3=\frac{e^2F_i^2}{2\hbar m_i^*}, \quad i=x,\,y,\,z.$$

The eigenvalue of the effective mass equation is $E=E_x+E_y+E_z$.

Since the asymptotic expansion of the Airy function yields an oscillatory function for negative arguments and an exponentially decaying function for positive arguments, Eq. (4), when replaced in the expression for ϵ_1 and ϵ_2 yields for a field along the x direction oscillations for $\hbar\omega$ above the energy gap and an exponential decay below it if $m_x>0$. The situation is reversed for a negative-mass direction. In cubic materials anisotropic masses, sometimes with different signs along the various principal directions, occur for critical points off $\mathbf{k}=0$. Because of the symmetry, one always has a number of equivalent critical points and hence a field which is along a principal direction of positive mass for one of the critical points, may be along a negative mass or a nonprincipal direction at another equivalent critical point. Oscillations can therefore result above and below the energy gap. Aspnes[31] has shown that the case of an electric field with components F_x, F_y, and F_z along the principal directions of the mass ellipsoid can be treated by using a reduced mass μ given by

$$\frac{1}{\mu}=\frac{1}{|F|^2}\left[\frac{F_x^2}{\mu_x}+\frac{F_y^2}{\mu_y}+\frac{F_z^2}{\mu_z}\right]. \qquad (6)$$

Oscillations occur above or below E_g depending on

[26] M. Cardona, Solid State Commun. **1**, 109 (1963)
[27] W. Franz, Z. Naturforsch. **13**, 484 (1958).
[28] L. V. Keldysh, Zh. Eksperim. i Teor. Fiz. **34**, 1138 [English transl.: Soviet Phys.—JETP **7**, 788 (1958)].
[29] J. Callaway, Phys. Rev. **130**, 549 (1963); **134**, A998 (1964).
[30] K. Thamarlingam, Phys. Rev. **130**, 2204 (1963).
[31] D. Aspnes, Phys. Rev. **147**, 554 (1966).
[32] R. J. Elliott, Phys. Rev. **108**, 1184 (1957).
[33] G. B. Duke, Phys. Rev. Letters **15**, 675 (1965).

whether μ is positive or negative. Because of the strongly nonlinear dependence of $\phi(0)$ on $\mathbf{F}$, when the effect of the various equivalent critical points are added, strong changes in shape of the spectra can result since the various critical points see a different reduced field $F_i/\mu_i^{1/2}$ [see Eq. (5)]. The period of the oscillations at one critical point is proportional to

$$|\psi^3|^{1/3}=\theta=\left|\frac{e^2|F|^2}{2\hbar\mu}\right|^{1/3}.$$

It has been shown by Aspnes[31] that the variations induced in ϵ_1 and ϵ_2 by the electric field can be expressed for all types of critical points in terms of only two universal functions F and G related to the Airy function Ai, a modified Airy function Bi irregular at infinity, and their derivatives. $\Delta\epsilon_1$ is proportional to $G(\zeta)$ at an M_0 edge, and an M_2 edge with $\mu>0$, to $G(-\zeta)$ for an M_3 edge, and an M_1 edge with $\mu<0$, to $F(\zeta)$ for an M_1 edge with $\mu>0$ and to $F(-\zeta)$ for an M_2 edge with $\mu<0$. $\zeta=(E_g-\hbar\omega)/\hbar\theta$. Both $\Delta\epsilon_1$ and $\Delta\epsilon_2$ have a peak very near E_g. This peak does not shift in energy with increasing field while all other oscillations shift in energy as the field is varied: their distance in energy to the energy gap E_g varies like

$$\theta=\left|\frac{e^2|F|^2}{2\hbar\mu}\right|^{1/3}.$$

From this consideration follows the possibility of determining energy gaps by observing the Franz-Keldysh oscillations provided one can decide which peak corresponds to E_g. The absence of a shift when the field is varied is, in principle, a good criterion for this assignment.

Because the E_g peak is nonsymmetric, broadening effects[34] introduce a shift in the position of this peak. The corresponding error in the determination of E_g is always considerably smaller than the width of the peak. The determination of E_g is also complicated by the fact that the quantity obtained from the analysis of the electroreflectance data is not $\Delta\epsilon_1(\mathbf{F})=\epsilon_1(\mathbf{F})-\epsilon_1(0)$ and $\Delta\epsilon_2(\mathbf{F})=\epsilon_2(\mathbf{F})-\epsilon_2(0)$ but rather $\epsilon_1(\mathbf{F}_M)-\epsilon_1(\mathbf{F}_m)$ and $\epsilon_2(\mathbf{F}_M)-\epsilon_2(\mathbf{F}_m)$ where $\mathbf{F}_M$ and $\mathbf{F}_m$ are the maximum and minimum average field applied to the material as a function of time.[35] If $F_M-F_m\ll F_M$ the observed modulations are proportional to the derivatives of ϵ_1 and ϵ_2 with respect to F. Figure 4 shows the universal functions

$$F\frac{d\epsilon_1}{dF}\frac{\omega}{C\theta^{1/2}} \quad \text{and} \quad \Delta\epsilon_1\frac{\omega}{C\theta^{1/2}}$$

as a function of $(E_g-\hbar\omega)/(\hbar\theta)$ for the case of an M_0 edge.[31] (C involves only physical constants and density of states effective masses). It is seen that while $\Delta\epsilon_1$ has the strongest oscillations for $\hbar\omega$ near E_g, $d\epsilon_1/dF$ has oscillations which grow as $\hbar\omega-E_g$ increases. This alerts us to the fact that the edge E_g might not yield the strongest peaks in the experimental data. For the sake of completeness, we have included in Fig. 4 the intermediate case $\epsilon_1(F_M)-\epsilon_1(F_m)$ for $F_M=\frac{3}{2}F_m$ as the universal function[36]:

$$\frac{[\epsilon_1(F_M)-\epsilon_1(F_m)]\omega}{C[\theta(F_m)]^{1/2}}.$$

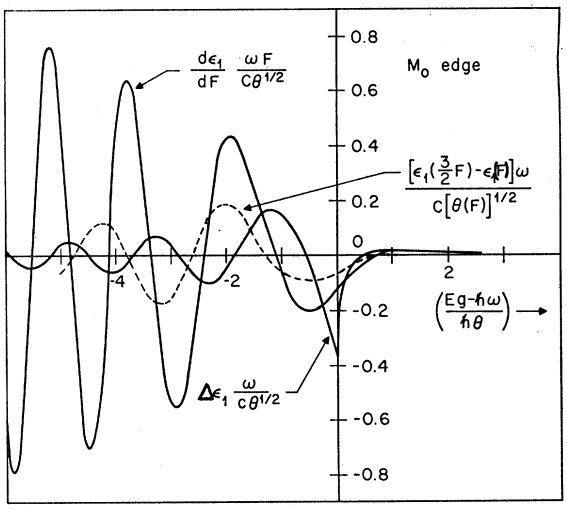

FIG. 4. Calculated spectral dependence of the universal functions $\Delta\epsilon_1(\omega/C\theta^{1/2})$, and $(d\epsilon_1/dF)(\omega/C\theta^{1/2})$ and $\frac{[\epsilon_1(\frac{3}{2}F)-\epsilon_1(F)]\omega}{C[\theta(F)]^{1/2}}$, representing the change induced in the dielectric constant ϵ_1 by a field F, the derivative of this change with respect to F, and the difference between the change induced by a field $\frac{3}{2}F$ and that induced by F. The curves correspond to an M_0 edge.

Figure 4 illustrates the fact that the shape of the experimental spectra should depend very critically on the relative values of F_M and F_m. A line shape variation as strong as that suggested by Fig. 4 is generally not encountered experimentally. Spectra of the derivative type, with oscillations growing as one moves away from E_g, are not observed even for very small modulation amplitudes. This may be due to broadening effects, disregarded in the Franz-Keldysh theory, and to the nonuniformity of the electric field which tends to dampen the oscillations as one moves away from E_g. Because of the difficulties outlined above and other inadequacies of the present theory (such as disregard of exciton effects), we shall not make an attempt at quantitively understanding the experimental line shapes. We shall only try to determine as well as possible

[34] B. O. Seraphin and N. Bottka, Phys. Rev. **145**, 628 (1966).

[35] This consideration strictly speaking only applies to square wave modulation. We have used square wave and sinusoidal modulations but no significant difference between them has been observed.

[36] We are grateful to Dr. D. Aspnes for performing the computer calculation of the derivative function in Fig. 4.

the energies of critical points from the position of the corresponding peaks in the electroreflectance spectra. These energies will be affected by the line shape errors discussed above.

The quantity directly measured in an electroreflectance experiment is the fractional change in reflectance $\Delta R/R$ produced by the applied modulating voltage. Because of the inhomogeneity of the field (for the Schottky barrier discussed in Sec. IV the field varies linearly with depth) an exact relationship between $\Delta R/R$ and the changes $\Delta\epsilon_1$, $\Delta\epsilon_2$ obtained from the theory is not easy to establish. Fresnel's equation for normal incidence reflectivity is not valid when the optical constants are a function of position. An exact expression would require at least a solution of the wave equation with continuously varying optical constants inside the semiconductor and possibly even the solution of the effective mass Schrödinger equation for the exact varying field. In order to avoid these complications, one can assume that Fresnel's equation for normal incidence reflectance applies provided one uses the optical constants obtained from the uniform field theory and equating this uniform field to some average field in the space-charge layer. This average field will, in general, be a function of wavelength since the penetration depth of the light varies with wavelength. We have not attempted to determine the proper type of field average to be used. This would not be of much relevance in the interpretation of our experiments since no attempt has been made to determine the magnitude of the modulation fields applied.

Once the validity of Fresnel's equation is postulated, it is easy to decompose[34] $\Delta R/R$ into the contributions from $\Delta\epsilon_1$ and $\Delta\epsilon_2$:

$$\frac{\Delta R}{R}=\alpha\Delta\epsilon_1+\beta\Delta\epsilon_2.$$

α and β can be easily calculated[34] if the optical constants of the sample and the electrolyte are known. Figure 5 shows α and β for germanium in an aqueous electrolyte assuming for water a nondispersive refractive index $n=1.33$. It is clear that near the fundamental edge E_0 the electroreflectance is dominated by $\Delta\epsilon_1$. Around E_1 the contributions of $\Delta\epsilon_1$ and $\Delta\epsilon_2$ are about equal and a small error in ϵ_1 and ϵ_2, of the order of that expected from a Kramers-Kronig analysis, can substantially alter the relative contributions of $\Delta\epsilon_1$ and $\Delta\epsilon_2$. The main contribution to the electroreflectance at the E_0' peak seems to come from $\Delta\epsilon_2$ while that at E_2 comes again from $\Delta\epsilon_1$ but the sign of $\Delta R/R$ is opposite to that of $\Delta\epsilon_1$.

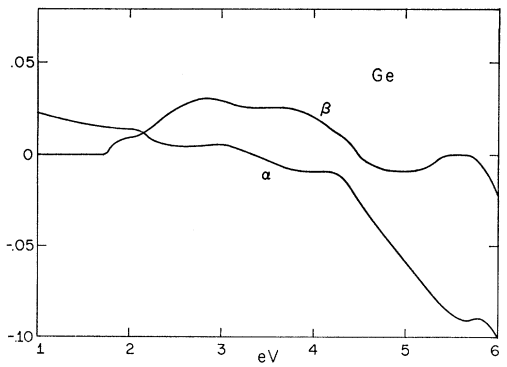

FIG. 5. Spectral dependence of the functions α and β governing the contribution of $\Delta\epsilon_1$ and $\Delta\epsilon_2$ to a reflectance modulation spectrum for a germanium sample immersed in water. α and β for germanium in air given in Ref. 34. ϵ_1 and ϵ_2 have been taken from Ref. 45.

Under the assumption that the reflectance at the space charge layer is caused by "average" optical constants which are functions of the layer voltage, it is possible to extract $\Delta\epsilon_1$ and $\Delta\epsilon_2$ from $\Delta R/R$ by using the Kramers-Kronig relations provided ϵ_1 and ϵ_2 are known. This will be done in Sec. VI.

IV. EXPERIMENT

A high electric field can be applied to an ideal insulator by simply placing it between condenser plates and applying a high voltage to them. Many of the insulators of interest are far from being ideal: their resistivity is finite and heating and breakdown effects limit the usefulness of the condenser method of applying high electric fields.

The depth of material contributing to the reflection of light in the region of direct interband absorption is of the order of the inverse of the absorption coefficient α. Since α lies typically between 10^4 and 10^6 cm^{-1}, the depth of material contributing to the reflection is 10^{-6} to 10^{-4} cm. The electric field required for the observation of electroreflectance can therefore be confined to a depth of the order of the penetration depth of the light. In a semiconductor the application of such a field can be readily accomplished in a lossless manner by using the field effect configuration.[4] The sample is used as one of the plates of a capacitor with a transparent dielectric (Saran Wrap in Seraphin's arrangement[4]) and a transparent conducting coating (SnO_2) as the other electrode. The ac voltage applied to the capacitor modulates the internal field at the surface of the semiconductor and produces a modulation of its reflectivity. This modulation can be easily detected with a lock-in amplifier.

The absorption edges of SnO_2 ($\sim$4 eV) and the dielectric foil determine the photon energy cutoff of the technique described above. A great deal of the structure observed in the reflection spectra of semiconductors occurs beyond 4 eV and hence this cutoff is a serious drawback. Mechanical vibrations in the capacitor structure produced by the modulating field may produce spurious signals.[37] Also, because of the complicated nature of the optical system, involving several reflecting

[37] Vibration effects were minimized by Seraphin [Phys. Rev. 140, A1716 (1965)] by wetting the various surfaces in contact with a mixture of Canada balsam and diffusion-pump oil.

surfaces, extraction of the changes induced by the electric field on the optical constants from the electroreflectance data (see Sec. VI) is nearly impossible.

In order to eliminate some of the drawbacks listed above we have applied the electric field by immersing the semiconductor in an electrolyte and biasing it in the reverse direction. The photon energy cutoff is now determined by the cutoff of water (~7 eV) and mechanical vibrations of the system do not occur since the capacitor structure is now mainly within the depletion layer of the semiconductor. The low-energy cutoff for conventional electrolytes is 1 eV. Also, owing to the absence of the dielectric foil (thick by comparison with a typical depletion layer), large modulations can be achieved with only a small modulating voltage (~1 V). Evaluation of the changes in optical constants is now easy since the only reflecting surface involved is the semiconductor-electrolyte interface. Irregularly shaped samples or samples cleaved within the electrolyte can be easily handled by this method.

The obvious disadvantage of the electrolyte technique is its temperature limitation: freezing and boiling of the water makes aqueous electrolytes useless below 0°C and above 100°C. Measurements down to −100°C can be readily performed using methanol (+KCl) or ethanol (+H_2SO_4) as the electrolyte. These electrolytes are also useful for measuring materials which react with or dissolve in water (e.g., AlSb). A diagram of our experimental setup is shown in Fig. 6.

The Electrolytic Cell

The semiconductor-electrolyte junction is built by immersing the sample in the electrolyte and biasing it with respect to a platinum electrode so as to form a blocking contact. For all materials measured, with the exception of silicon and GaAs, blocking contacts are only obtained when the sample is biased negatively, regardless of its type (see Fig. 7). Blocking contacts, and hence electroreflectance signals, were obtained in silicon and GaAs for both bias directions: This effect

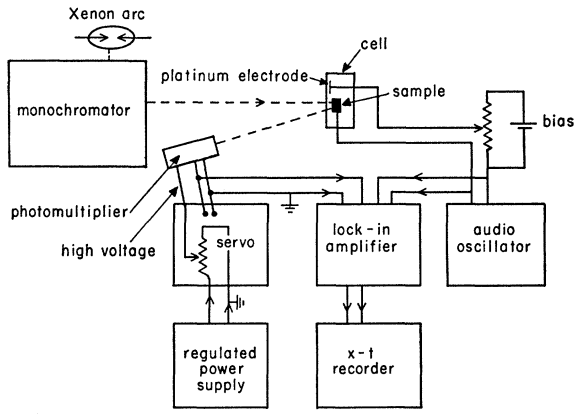

FIG. 6. Experimental setup used for electroreflectance spectroscopy.

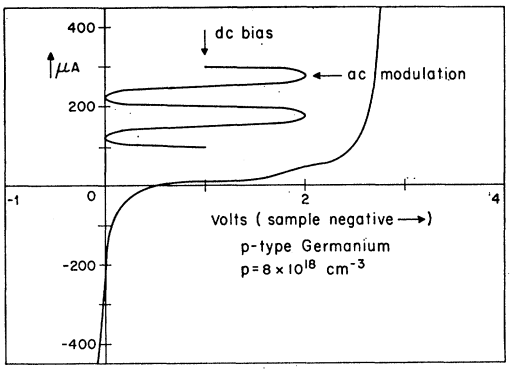

FIG. 7. I–V curve of a p-type germanium sample with $p=8\times10^{18}$ cm^{-3}.

is probably related to the presence of an oxide at the surface.

In order to obtain the reflectance modulation, an ac voltage is added to the dc bias. The sum of the dc bias and the ac modulating voltage at the semiconductor-electrolyte interface must be kept lower than the voltage at which strong conduction sets in (breakdown voltage, see Fig. 7). Typical dc bias voltages for aqueous electrolytes (see below) are of the order of 1 V and the corresponding current densities 10 μA/cm^2. Modulation voltages are also of the order of 1 V. A cell with a quartz window was used for room temperature measurements. A quartz Dewar with a silver-free circular strip was used at low temperatures: the electrolyte was cooled through a heat leak from a liquid nitrogen bath and the temperature was regulated by means of a resistance heater.

Making electrical contact to the sample presents no problem since the contact does not have to be of very low resistance. The contact resistance should be small compared with that of the semiconductor-electrolyte interface but contact resistances of the order of that of the interface can be tolerated provided higher dc and ac voltages are applied to the cell. Pressed contacts were made in most cases on a dot of Dupont No. 4817 silver paint painted on the sample. When large samples were available the contact was made at one edge of the sample and kept above the electrolyte level. Small samples were glued with silver paint to a brass rod and potted with epoxy so as to exhibit only the surface to be measured.

The thickness of the space-charge layer X in the semiconductor is obtained in the complete depletion approximation[38] by integrating Poisson's equation with a charge density equal to the bulk carrier density N times the charge of the electron e:

$$X=\left(\frac{\epsilon V}{2\pi Ne}\right)^{1/2}, \tag{7}$$

[38] J. T. Law, in *Semiconductors*, edited by N. B. Hannay (Reinhold Publishing Company, New York, 1959), p. 682.

where V is the voltage seen by the depletion layer and ϵ the static dielectric constant of the material. The average field at the surface layer is $\langle E\rangle = V/X$. Typical values of X and $\langle E\rangle$ are, for $V=1$ V and $N=10^{17}$ cm^{-3}, $X=10^{-5}$ cm and $\langle E\rangle = 10^5$ V$\times$cm^{-1}. The penetration depth of the field varies like $N^{-1/2}$ and hence a wide range of lower concentrations is acceptable for measurements. We have seen electroreflectance spectra in samples with N as low as 10^{14} cm^{-3} and as high as 10^{20} cm^{-3}. The carrier concentration which gives the largest signals lies, in general, somewhere around 10^{18} cm^{-3}.

The electroreflectance spectra do not depend critically on the solute concentration in the electrolyte. In order to obtain large signals it is advisable to keep the ion concentration high enough so as to have the space-charge layer in the electrolyte (Gouy layer) thinner than the corresponding layer in the semiconductor. Under these conditions, the voltage drop at the Gouy layer is negligible. This is readily achieved with aqueous electrolytes (e.g. 1 molar KCl in water) for semiconductors with $N \lesssim 10^{19}$ carriers$\times$cm^{-3}. With methyl or ethyl alcohol such high ionic concentrations cannot be obtained and a large voltage drop is produced at the Gouy layer. In order to obtain large signals, the applied ac and dc voltages must be increased. Typical values of these voltages for KCl in methanol are around 5 V.

The modulation frequencies used lay between 30 and 300 cps. As the frequency is increased a decrease in the reflectance modulation is sometime observed. It is due to the increase in capacitive admittance of the space charge layer which produces an increase in the ac current and hence a voltage drop due to losses at the contact and at the electrolyte. The original amount of signal can be easily recovered by increasing the modulation voltage.

The voltage V in Eq. (7) is the sum of the built-in junction voltage and the portion of the applied voltage seen by the space-charge layer. Because of the screening effect of the large density of surface states present, the space-charge layer sees only a small fraction of the applied voltage. This is particularly true for the dc bias since the slow surface states are fully effective in screening it. The ac modulation is not as effectively screened by the slow surface states. We have not attempted to estimate the modulation fields involved in our experiment. Such an estimate can be made by means of field effect measurements.[39]

Sample-Surface Preparation

For the preparation of the reflecting surfaces the various techniques known to give sharp and reliable reflectivity spectra were used. Surfaces of growth and cleaved surfaces were used and also mechanically polished surfaces followed by chemical etching.[40] All mechanically polished surfaces were given a final polish with Linde B levigated alumina. For the polished samples the quality (magnitude and sharpness) of the spectra obtained was far more dependent on the fact that the surface had been etched than on the optical quality of the surface itself. Highly polished and etched surfaces and dull etched surfaces often gave quite similar results. Many cleaved surfaces were far from flat but still gave good results. The pertinent information about the samples used in the measurements reported here is given in Table I.

TABLE I. List of samples and surface treatments used for the electroreflectance measurements.

Material	Type	Carrier concentration cm^{-3}	Surface preparation
Si	n and p	$10^{15}-10^{20}$	etched HNO_3-HF-CH_3COOH 25:15:15
Ge	n and p	$10^{14}-10^{20}$	etched HNO_3-HF 1:1
α-Sn	n	unknown	surface of growth from mercury solution
AlSb	p	unknown	cleaved in methanol
GaP	n	2×10^{16}	etched HCl-HNO_3 1:1
GaAs	n and p	$10^{15}-10^{19}$	etched HCl-HNO_3 1:1 or Br_2-CH_3OH 1:10
GaSb	n	10^{18}	etched Br_2-CH_3OH 1:10
InP	n	10^{16}	etched HCl-HNO_3 1:1
InAs	n	unknown	etched Br_2-CH_3OH 1:10
InSb	n	10^{16}	etched Br_2-CH_3OH 1:10
ZnO	n	unknown	surface of growth from vapor phase
ZnTe	p	unknown	cleaved
CdS-cubic	n	unknown	surface of epitaxial growth
CdS-hex	n	unknown	cleaved
CdSe	n	unknown	cleaved, also etched
CdTe	n	unknown	etched HF-H_2O_2-H_2O 20:15:10
HgSe	n	unknown	etched HNO_3-CH_3COOH-H_2SO_4-HCl 50:10:20:1
HgTe	n	unknown	cleaved

Optical System

Since the signal-to-noise ratio is proportional to the square root of the light intensity, an intense light source and a large aperture monochromator are necessary in order to obtain high sensitivity. We have used as a light source an XBO 450 Osram Xenon arc (450W) or a 970C1 Hanovia arc throughout the whole spectral region of measurement (1–6 eV). Quartz-iodine tungsten-filament lamps (sun guns) such as Sylvania DW (600 W) are also quite suitable in the 1–3.5 eV region. Monochromatic light was produced with a Bausch and Lomb 50 cm grating monochromator. Its resolution limit ($\sim$10 Å) is sufficient for the structure observed in the electroreflectance spectra of all materials measured. Commercial-grade quartz lenses were used to focus the light on the sample and on the photomultiplier. We believe they are responsible for the 6-eV photon energy

[39] T. M. Donovan and B. O. Seraphin, J. Electrochem. Soc. **109**, 877 (1962).

[40] H. C. Gatos and M. C. Lavine, in *Progress in Semiconductors*, edited by A. F. Gibson and R. E. Burgess (Temple Press, London, 1965), Vol. 9, p. 1.

cutoff of our system. Suprasil lenses and Xenon arcs with suprasil envelopes (Hanovia 970C1 Special) should extend the photon energy of our system for unpolarized light to 7 eV. A glan prism with air gap was used as a polarizer for the measurements with polarized light.

As a detector for the visible and infrared we used a Dumont 6911 photomultiplier (S1 response). For the uv and visible we used an EM1 6256B tube (S13 response). The measurements were performed at nearly normal incidence (angle of incidence $\sim 10°$) and care was taken to eliminate the reflection from the front window by mounting the sample surface at an angle with it.

Electronics

The block diagram of the electronic equipment used is shown in Fig. 6. We used as lock-in amplifiers PAR models HR8 and JB5[41] and an EMC[42] model RJB unit. The wavelength was swept with a syncronous motor and the signal displayed on a Heathkit strip-chart recorder. An accurate wavelength marker consisting of a slotted wheel connected to the wavelength drum, an incandescent bulb and a photorelay which shorted out the recorder input, enabled us to determine the wavelength to ± 2 Å.

One of the most attractive features of reflectance modulation experiments is the fact that two signals are detected by the photomultiplier: a dc signal proportional to the average reflectivity R and an ac signal proportional to the reflectivity modulation ΔR. By dividing the ac by the dc signal the quantity $\Delta R/R$ is directly obtained independent of the incident intensity. This feature eliminates the cumbersome moving parts involved in determining the incident intensity in standard reflectivity measurements. It also automatically corrects for fluctuations in the intensity of the light source, a common handicap in high-pressure arcs. Several schemes have been devised to obtain the ratio of the two signals mentioned above.[2,4,6] We apply the dc output from the photomultiplier to a servomechanism acting on a voltage divider which varies the high voltage applied to the photomultiplier. The high voltage is varied so as to keep the dc output constant ($=1$ V). Under these conditions the ac output from the lock-in amplifier is proportional to the ratio $\Delta R/R$.

V. RESULTS

A. Group-IV Elements

Germanium

Figure 8 shows the room-temperature electroreflectance spectrum of n-type germanium ($N=4.5\times10^{14}$ cm^{-3}). Electroreflectance spectra were obtained

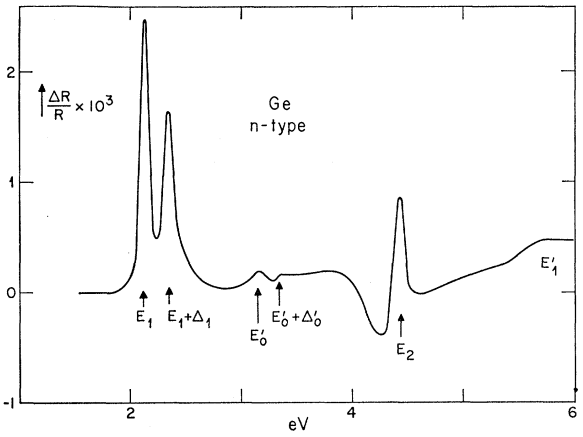

FIG. 8. Electroreflectance spectrum of n-type germanium with 5×10^{14} electrons cm^{-3} at room temperature. $V_{dc}=1.5$ V, $V_{ac}=1$ V rms. Due to the small doping and the position of the Fermi level at the surface, the sign of the electroreflectance peaks is the same as observed in p-type material. In this and all subsequent figures the sign of ΔR is that observed when the negative cycle of the modulating voltage is applied to the sample.

in germanium only when the sample was negatively biased with respect to the platinum electrode. The lock-in amplifier was tuned at the fundamental frequency of the modulating field. Since the Franz-Keldysh effect is even in the electric field, the observation of a signal at the fundamental frequency requires the presence of an internal dc field at the surface. The phase of the signal depends on the sign of this internal field. It was found for most materials measured that the phase of the peaks reverses when reversing the sign of the charge carriers. This indicates that the Fermi level at the surface is near the center of the forbidden gap[43]: the signal at the fundamental frequency reverses sign at the doping which corresponds to flat bands at the surface. The situation is different if observations are made at the second harmonic of the modulating frequency: the phase of the observed signal is independent of the type of doping.

The sign of the peaks shown in Fig. 8 is that characteristic of p-type germanium samples. While the sample is n-type, its carrier concentration (5×10^{14} cm^{-3}) is near intrinsic at room temperature (10^{14} cm^{-3}) and the bulk Fermi level is quite close to the center of the gap. At the surface the Fermi level must be closer to the bottom of the conduction band than to the valence band so as to produce an internal field of the same sign as in p-type material. We thus conclude that the Fermi level at the surface lies *above* the center of the forbidden gap. Since samples with $N=10^{18}$ cm^{-3} have peaks of phase opposite to those of p-type samples, the Fermi level at the surface must be below the bottom of the conduction band. This conclusion is only valid for germanium surfaces in contact with water.[43]

Several of the peaks observed in the reflection spec-

[41] Princeton Applied Research Corporation, Princeton, New Jersey.

[42] Electronics, Missiles, and Communications, Mount Vernon, New York.

[43] C. A. Mead and W. G. Spitzer, Phys. Rev. **134**, A713 (1964).

trum of Fig. 1 are seen with much better resolution in Fig. 8. The direct absorption edge (E_0, $E_0+\Delta_0$) does not appear in Fig. 8 because of the opacity of water to the corresponding photon energies. The electroreflectance peaks due to these transitions have, however, been observed by the technique of Seraphin and Hess.[4] The E_1 peak and its spin-orbit split $E_1+\Delta_1$ are better resolved in Fig. 8 than in Fig. 1. While these peaks are not the strongest in the conventional reflection spectrum they are the strongest structure observed in the electroreflectance.

No indication has been obtained in the electroreflectance spectrum of the e_1, $e_1+\Delta_1$ peaks observed by Potter[18] slightly below E_1 and $E_1+\Delta_1$ and attributed to transitions at the L point ($L_3' \rightarrow L_1$). The E_0' peak is seen around 3.2 eV with an indication of a splitting Δ_0' of about 0.18 eV. A similar but somewhat stronger set of peaks is seen for all III–V compounds: the splitting Δ_0' is always slightly less than the Δ_1 splitting.[44] The correlation between Δ_0' and Δ_1 enables us to infer that Δ_0' is also produced by the spin-orbit interaction. A tentative assignment of E_0' and $E_0'+\Delta_0'$ is given in the discussion.

An s-shaped peak is seen at 4.27–4.42 eV. The sharpness and strength of the 4.4-eV component and the small variation of its position with voltage and doping suggests that it is the leading peak of the structure. The 4.27-eV swing is probably a satellite oscillation although we cannot altogether discard its being produced by another critical point near the 4.42 eV gap. Some indication of the E_1' structure is seen towards the high energy end of the spectral range in Fig. 8. It is however, too ill-defined for any specific discussion.

Figure 9 shows the electroreflectance spectrum of two heavily doped germanium samples ($N=4.5\times10^{19}$ cm^{-3}, $P=2.4\times10^{20}$ cm^{-3}). This figure demonstrates the reversal of the peaks from n- to p-type material. All of the structure observed in purer germanium appears also in Fig. 9 but the two components of the E_0' peak are not resolved. The E_2 peak is not broadened much by the doping. E_1 and $E_1+\Delta_1$ are considerably broadened and their strength is decreased relative to that of E_2. We believe this is due to the small penetration depth (~50 Å) of the surface field in these heavily doped materials. This penetration depth almost exactly matches that of the light at the E_2 energy (the absorption coefficient[45] α is 2×10^6 cm^{-1} at 4.4 eV) while the light penetrates considerably more than the field (~200 Å) around E_1 and $E_1+\Delta_1$. The "average" electric field which contributes to the Franz-Keldysh effect is smaller at E_1, $E_1+\Delta_1$ than at E_2 and the relative strengths of the corresponding peaks can thus be explained.

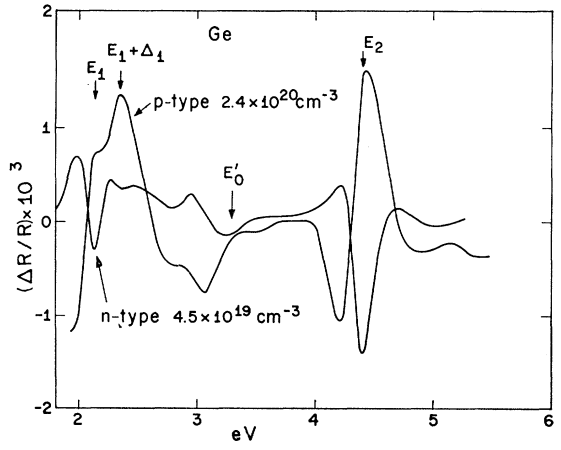

FIG. 9. Electroreflectance spectrum of two heavily doped germanium samples ($V_{dc}=1$ V, $V_{ac}=0.2$ V rms). Unless otherwise specified all data presented in this paper were taken at room temperature.

Another phenomenon apparent in Fig. 8 is the change of the relative intensities of the E_1, $E_1+\Delta_1$ peaks. In pure and heavily doped n-type samples E_1 is stronger than $E_1+\Delta_1$. In the p-type sample of Fig. 9, $E_1+\Delta_1$ is much stronger than E_1. This reversal does not occur for $P=6\times10^{19}$ cm^{-3} at room temperature. A possible explanation of this phenomenon will be given in Sec. VII.

Table II shows the energies of the E_1, $E_1+\Delta_1$, E_0', $E_0'+\Delta_0'$, and E_2 peaks found in the electroreflectance spectrum of some germanium samples. The position of the various peaks in a given spectrum can be determined, at least for the purer samples, with an accuracy of 2 meV. Because of irreproducibility for different runs and samples (no detailed study of the small influence of surface orientation and other factors on peak energies was made) we have given only two decimal places for the energies of the peak. An unambiguous dependence of the energy of the peaks on doping was not observed. A decrease of 0.03 eV for the heaviest dopings has been observed[46] in the E_1 reflection

TABLE II. Positions of the electroreflectance peaks (in eV) observed for several germanium samples. The dc bias and ac modulation voltages at which the experiments were performed are also given.

Type	Carrier concentration cm^{-3}	V_{dc} (V)	V_{ac} (V rms)	E_1 (eV)	$E_1+\Delta_1$ (eV)	E_0' (eV)	$E_0'+\Delta_0'$ (eV)	E_2 (eV)
n	5×10^{14}	1.5	1	2.12	2.34	3.14	3.33	4.42
p	10^{16}	1.5	0.6	2.14	2.35	3.15	3.34	4.41
n	8×10^{18}	1.5	0.25	2.11	2.35	3.17	3.32	4.40
n	4.5×10^{19}	1	0.2	2.12	2.36	3.25		4.40
p	8×10^{19}	1	0.2	2.13	2.33	3.33		4.42
p	2.4×10^{20}	1	0.2	2.11	2.35	3.31		4.44

[44] K. L. Shaklee, M. Cardona, and F. H. Pollak, Phys. Rev. Letters **16**, 48 (1966).

[45] H. Ehrenreich and H. R. Philipp, Phys. Rev. **129**, 1550 (1963).

[46] M. Cardona and H. S. Sommers, Jr., Phys. Rev. **122**, 1382 (1961).

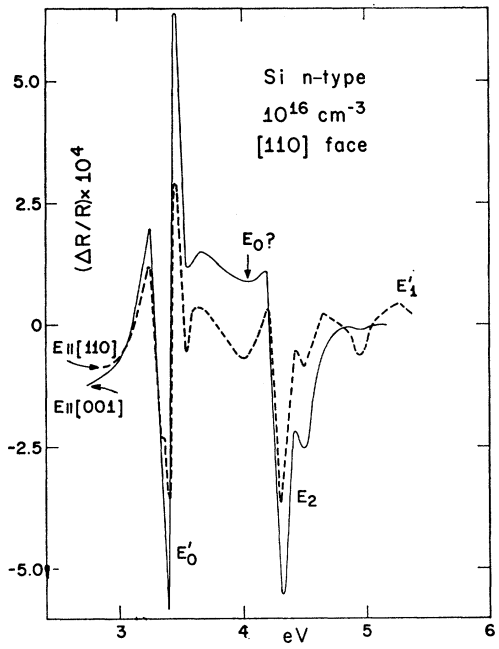

FIG. 10. Electroreflectance spectrum of n-type silicon at room temperature. Surface orientation [110]. Electric field of the light polarized parallel to [001] and parallel to [$\bar{1}$10]. $V_{dc}=+3$ V (sample positive) so as to keep the Fermi level at the surface *below* that of the bulk (n-type peaks). $V_{ac}=4$ V rms.

peak. Such a decrease is compatible with the data in Table II.

Silicon

Silicon differs from most of the materials measured (except GaAs and GaP) in that electroreflectance signals are obtained for either positive, zero, or negative dc biases. We believe this peculiarity is due to the formation on the silicon surface of an oxide layer which prevents direct contact of the electrolyte with the silicon: in order to obtain signals of the same magnitudes as in germanium much higher modulating voltages are necessary. Also, in all samples measured with the exception of heavily doped p type, it was possible by varying the sign and magnitude of the dc bias to invert the phase of the peaks and thus go from n-like to p-like spectra (see Table III). This phenomenon is illustrated in Figs. 10 and 11. The spectrum in Fig. 10 was obtained with a dc bias of +3 V (sample positive) and is n-like: the band-edge energies at the surface are *above* those of the bulk. The bias in Fig. 11 is −3 V and the spectrum is p like. Actually the spectra of all n-type samples measured were p like when no dc bias was applied. This indicates that the Fermi level at the surface is, with no bias applied, above the bottom of the conduction band.

The reflecting surface used for the measurements of Figs. 10 and 11 was cut perpendicular to the [110] axis. The electroreflectance spectrum for this sample orientation should depend on the direction of polarization of the incident light, while that of a (111) or a (100) surface should not. Hence we have measured the (110) surface for the two normal modes of light polarization: **E** parallel to [001] and parallel to [1$\bar{1}$0]. The anisotropy of the effect is apparent: the E_0' and E_2 structures are much stronger for **E**∥[001] than for **E**∥[1$\bar{1}$0], the structure around 5.4 (corresponding to the E_1' reflection structure) is weaker for **E**∥[001]. Moreover, the peak around 3.4 eV (E_0') appears split into 3.32–3.38 eV for **E**∥[1$\bar{1}$0] direction and not for **E**∥[001].

TABLE III. Positions of the electroreflectance peaks (in eV) observed for several silicon samples. The measurements were performed with positive and with negative dc bias. The phase of the observed peaks (p or n like) is also tabulated.

Type	Carrier concentration cm^{-3}	V_{dc} (V)	V_{ac} (V rms)	Phase of peaks	E_0' (eV)	E_2 (eV)	
n	10^{16}	+3	4	n	3.39	4.31	4.51
n	10^{16}	−3	4	p	3.45	4.34	4.56
p	10^{16}	+3	2	n	3.40	4.32	4.50
p	10^{16}	−3	2	p	3.42	4.34	4.54
p	3×10^{19}	+3	1	p	3.40	4.32	4.47
p	3×10^{19}	−3	1	p	3.40		
n	6×10^{19}	+1	1	n	3.39	4.40	
n	6×10^{19}	+3	1	p	3.48	4.40	4.60

Following the customary notation[10] we have labeled the 3.4-eV peak E_0'. Electroreflectance measurements on germanium-silicon alloys[47] actually indicate that a superposition of the peaks corresponding to E_0' and E_1 of germanium occurs near 3.4 eV for silicon. The direct edge E_0 of germanium can also be followed with increas-

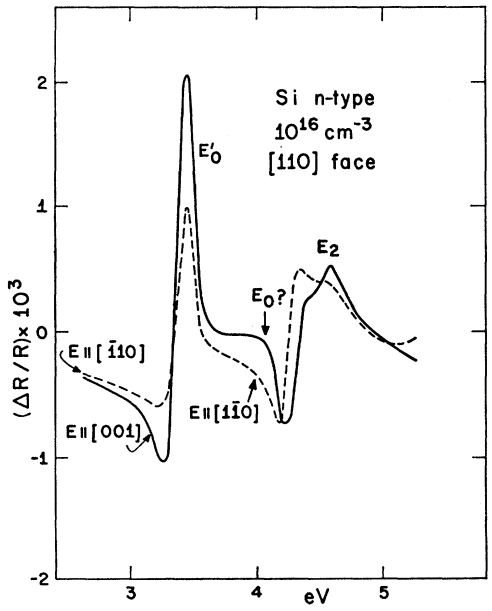

FIG. 11. Electroreflectance spectrum of the sample of Fig. 10. All conditions were kept the same as in Fig. 10 except the dc bias which was −3 V (sample negative).

[47] M. Cardona, K. L. Shaklee, and F. H. Pollak (to be published).

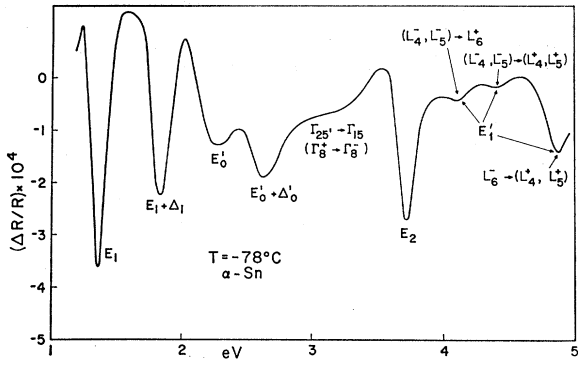

FIG. 12. Electroreflectance spectrum of gray tin at −78°C. $V_{dc}=1.5$, $V_{ac}=4$ V rms.

ing silicon content in the alloys system up to about 50% silicon[47]: it extrapolates linearly to 4.05±0.1 eV in silicon. The structure near 4 eV in Figs. 10 and 11, possibly satellite structure of E_2, could also be due to the E_0 peak of silicon.

The E_2 structure (see Table III) exhibits two components (4.31 and 4.51 eV in Fig. 10). Two components can also be seen barely resolved in the reflection spectrum at 4.3 and 4.5 eV.[48] We have lised in Table III the position of the E_0' and E_2 electroreflectance peaks observed in several silicon samples together with their phase (n or p like). The p-like peaks occur at slightly higher energy than the n-like peaks for a given sample.

Gray Tin

Figure 12 shows the electroreflectance spectrum of an n-type gray tin crystal prepared by the Ewald technique.[49] A discussion of these measurements has been published elsewhere.[50] The E_1, $E_1+\Delta_1$ structure is well resolved (1.365±0.002, 1.845±0.004 eV). The E_2 peak is similar to that of germanium: it is not split like in silicon. The splitting of the E_0' structure is clearly resolved thus confirming its spin-orbit origin (the spin-orbit interaction is larger in gray tin than in germanium). There is some question as to whether the shoulder labeled $\Gamma_{25'}-\Gamma_{15}$ corresponds to a gap or is simply satellite structure. The E_1' structure is now well within the range of our technique and is resolved into three components (4.11, 4.39, and 4.89 eV).

B. III–V Compounds

GaAs

The electroreflectance spectrum of GaAs near E_0 and E_1 has already been reported by Seraphin.[51] We have studied the electroreflectance spectrum of this material as a function of carrier concentration, dc bias and modulating voltage. Such extensive study has not been conducted for other III–V compounds. The peaks observed were n-like for all n-type samples measured ($N\gtrsim 5\times10^{15}$ cm^{-3}) and p-like for all p-type samples ($P\gtrsim 10^{16}$ cm^{-3}). We may therefore conclude that the Fermi level at the surface is inside of the forbidden gap and close to its center.

Lines due to impurity levels have been reported[51] at energies lower than the E_0 gap in the electroreflectance spectrum of GaAs. These lines disappear in heavily doped samples: the discrete impurity levels merge with the associated bands. We have observed three types of impurity levels in GaAs: typical spectra of these levels are given in Fig. 13. Figure 13(a) shows the spectrum near E_0 of an n-type sample with $N=6\times10^{15}$ cm^{-3} not intentionally doped. The direct gap E_0 ($E_0=1.430$ eV at room temperature according to Sturge[52]) is only seen for small modulating voltages. For larger modulating voltages ($V_{ac}\gtrsim 0.24$ V rms) only the impurity peak E_I is seen. From the separation between E_I and E_0 we infer that the ionization energy of the impurity responsible for E_I is 0.020±0.005 eV. Extensive electroreflectance measurements have been performed as a function of uniaxial stress[9] for the samples of Fig. 13(a). The impurity peak E_I shifts linearly with pressure in a manner similar to E_0. Since nonlinearities would be expected for an impurity level tied to the top of the valence band,[53] we believe that the level responsible for E_I is close to the bottom of the conduction band. Figure 13(b) shows the E_0, E_I peaks of a tellurium-doped n-type sample ($N=10^{17}$ cm^{-3}). A dependence on V_{ac} similar to that of Fig. 13(a) is apparent but, due to the higher ionization energy (0.045±0.005 eV), the values V_{ac} necessary to eliminate the E_0 peak are higher (2 V rms). We have not done uniaxial stress experiments on the samples of Fig. 13(b) and hence we cannot

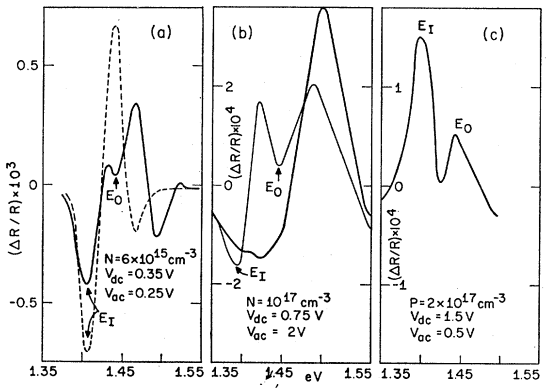

FIG. 13. Electroreflectance spectra of several GaAs samples showing impurity effects (E_I) near the fundamental edge (E_0).

[48] F. Lukeš and E. Schmidt, in *Proceedings of the 7th International Conference on the Physics of Semiconductors, Paris, 1964* (Dunod Cie, Paris, 1964), p. 197.
[49] A. W. Ewald and O. N. Tufte, J. Appl. Phys. **29**, 1007 (1958).
[50] M. Cardona, P. McElroy, F. H. Pollak, and K. L. Shaklee, Solid State Commun. **4**, 319 (1966).
[51] B. O. Seraphin, Proc. Phys. Soc. (London) **87**, 239 (1966).
[52] M. Sturge, Phys. Rev. **127**, 768 (1962).
[53] P. J. Price, Phys. Rev. **124**, 713 (1961).

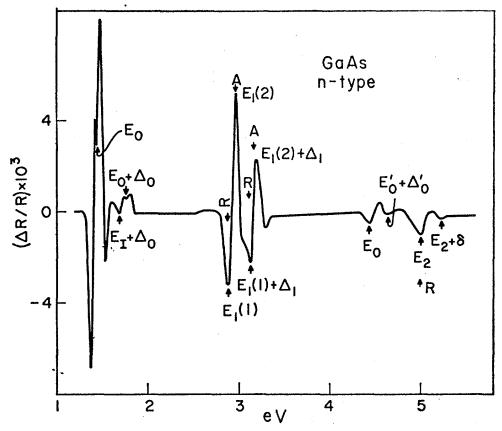

FIG. 14. Electroreflectance spectrum of n-type GaAs ($N=10^{17}$ cm^{-3}). $V_{dc}=1$ V, $V_{ac}=1$ V rms. The positions of some of the peaks observed in conventional reflection and absorption spectra are indicated as R and A in this figure.

conclude with certainty whether the level is tied to the conduction or to the valence band. For these types of samples an impurity peak is also associated with the $E_0+\Delta_0$ spin-orbit split peak ($E_I+\Delta_0$ in Fig. 14). As V_{ac} and V_{dc} are varied, the ratio of the intensities of E_I and E_0 remains the same as that of $E_I+\Delta_0$ and $E_0+\Delta_0$. We believe this indicates that the impurity level is tied to the conduction band. While the possibility of the $E_I+\Delta_0$ peak being caused by transitions from a level tied to the spin-orbit split valence band cannot be discarded, the ratio of the intensities of $E_I+\Delta_0$ and $E_0+\Delta_0$ should not be the same as that of E_I and E_0 due to the different population of the impurity levels tied to the Γ_8 and to the Γ_7 bands (Fig. 3).

Figure 13(c) shows the E_I-E_0 peaks of p-type GaAs (zinc doped, $P=2\times10^{17}$ cm^{-3}). The E_0 peak only appeared for a few minutes after applying the dc voltage. As time went on E_0 disappeared but it could be easily recovered turning V_{dc} off and on again. The impurity ionization energy is 0.03 ± 0.005 eV, similar to that observed in other optical experiments with similar samples.[54,55] We believe piezo-electroreflectance measurements[9] on these samples will settle the question of whether the impurity level is tied to the valence or to the conduction band.

The remaining structure in Fig. 14 has already been discussed[56] in connection with measurements of the GaAs–GaP alloys. There is some question as to whether the first or the second swing of the E_1, $E_1+\Delta_1$ peaks is more representative of the position of the corresponding gap: the first (1) swings occur closer to the reflectance peak while the second (2) are closer to the peaks in absorption.[57] A comparison of the E_1, $E_1+\Delta_1$ line shapes with theoretical calculations[31,34] indicates that the gaps are somewhere between the (1) and (2) peaks if broadening is included. We feel, however, that the (1) swing is closer to the gap since it has the same sign as the dominant E_1, $E_1+\Delta_1$ peaks of germanium of the same type (n-like peaks are only obtained for n-type germanium of $N\gtrsim10^{18}$ cm^{-3}). Also, $E_1(1)$ and $E_1(1)+\Delta_1$ are less sensitive to field[51] and doping (see Fig. 15) than $E_1(2)$ and $E_1(2)+\Delta_1$.

Figure 15 shows the dependence on doping of the electroreflectance peaks of GaAs (except E_0, $E_0+\Delta_0$ and impurity peaks). The increase in energy of $E_1(1)$, $E_1(2)$, $E_1(1)+\Delta_1$, $E_1(2)+\Delta_1$ can be explained as due to the increase in the internal field with doping. The fact that similar increases are found for n- as for p-type material of the same doping indicates that the Fermi level at the surface is near the center of the forbidden gap. The scatter of the points gives a good idea of the reproducibility and thus of the accuracy of the data (±0.01 eV for the peaks of the E_1 and E_0' families at low dopings, ±0.01 eV for E_2, and ±0.03 eV for $E_2+\delta$). No doping (field) dependence is found for E_0', $E_0'+\Delta_0'$, E_2, and $E_2+\delta$ thus confirming the contention that they are gap structure rather than satellites.

Figure 16 shows the electroreflectance spectrum of 2 heavily doped n- and p-type GaAs samples. While the structure above 2 eV is essentially the same (except for a slight broadening) as that observed in the less-doped sample (Fig. 14), the fundamental edge structure (E_0, $E_0+\Delta_0$) is considerably different. In both samples the E_0 peak has shifted towards higher energies. A definite shift towards higher energies is also seen for $E_0+\Delta_0$ in the n-type sample. Similar shifts, usually called Burstein-Moss shifts, are also observed in the conventional absorption spectra.[54] Their origin is the shift in the occupation by the free electrons/holes of the lower/higher states in the conduction/valence band,

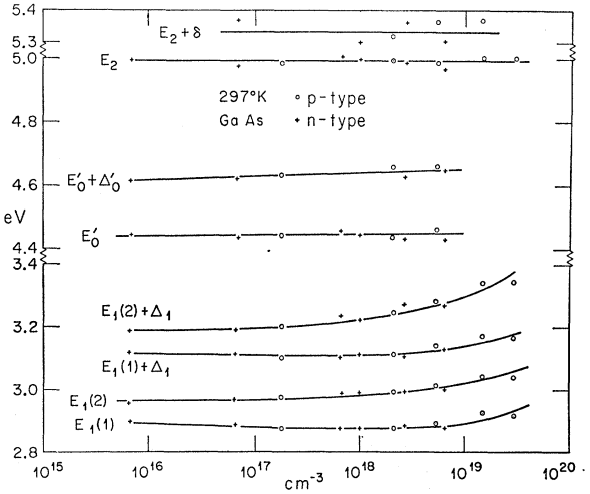

FIG. 15. Dependence on doping of the energy of the peaks observed in the electroreflectance spectrum of GaAs.

[54] J. Pankove, Phys. Rev. **140**, A2059 (1965).
[55] M. I. Nathan and G. Burns, Appl. Phys. Letters **1**, 98 (1962).
[56] A. G. Thompson, M. Cardona, K. L. Shaklee, and J. C. Woolley, Phys. Rev. **146**, 601 (1966).
[57] M. Cardona and G. Harbeke, J. Appl. Phys. **34**, 813 (1963).

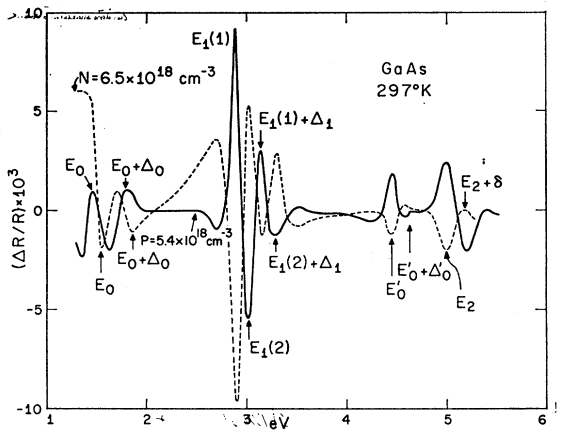

FIG. 16. Electroreflectance spectra of two heavily doped GaAs samples ($N=6.5\times10^{18}$ cm^{-3} and $P=5.4\times10^{18}$ cm^{-3}).

thus preventing these states from taking part in optical transitions. For completely degenerate material the transitions of the optical edge occur at points of **k** space on the Fermi surface. Hence, the edge occurs at an energy $E_g+E_F+E(k_F)$ where E_g is the gap of undoped material, E_F the Fermi level with respect to the bottom of the band occupied by free carriers and $E(k_F)$ the energy corresponding to momentum k_F (the Fermi momentum) in the band without free carriers. A Burstein-Moss shift is expected for $E_0+\Delta_0$ in n-type but not in p-type material.

Figure 17 shows the energies by which the E_0 (and some $E_0+\Delta_0$) peaks exceed the undoped gap as a function of doping in n- and p-type GaAs. Also plotted in Fig. 17 is the calculated Fermi levels of n-type[58] and

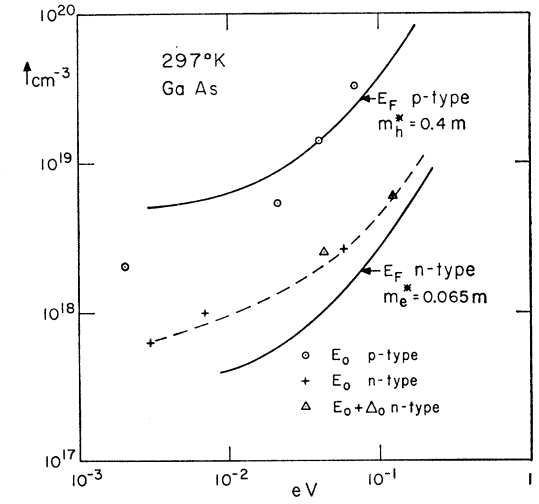

FIG. 17. Burstein-Moss shift of GaAs as a function of carrier concentration, as found in the electroreflectance spectrum at room temperature. The calculated curves include nonparabolicity effects in n-type but not in p-type material.

[58] M. Cardona, Phys. Rev. **121**, 752 (1961).

p-type material. In n-type material $E(k_F)$ is negligible for transitions originating at the heavy hole band. Thus the experimental points in Fig. 17 agree reasonably well with E_F for n-type GaAs. Hence, the corresponding transitions either originate at the heavy hole band or, if they originate at the light hole band, do not obey **k** conservation. The experimental values of E_F are actually somewhat smaller than the calculated ones and this may indicate a shrinkage of the gap with doping.[54] However, since no theory of the E_0 line shape in heavily doped materials is available, we cannot say with certainty that the energy of the E_0 maximum corresponds to $E_g+E_F+E(k_F)$. Line-shape effects may also be partly responsible for the discrepancies between the theoretical E_F and the position of the E_0 electroreflectance peak.

For p-type material $E(k_F)$ is quite large. If direct transitions were predominant, practically the same Burstein-Moss shifts would be observed for n- as for

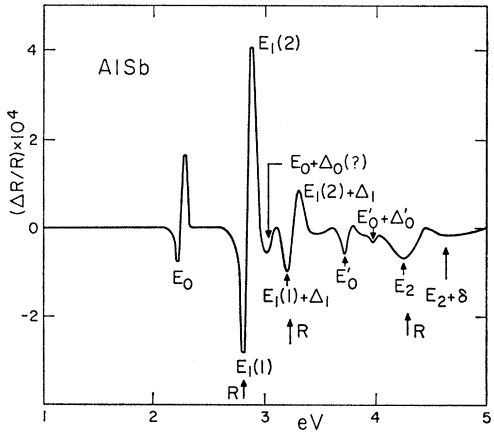

FIG. 18. Electroreflectance spectrum of p-type AlSb in methyl alcohol-KCl. $V_{dc}=4$ V, $V_{ac}=6$ V rms.

p-type material. Figure 17 actually shows that the Burstein-Moss shift agrees reasonably well with the Fermi level at the valence band. This fact suggests that the gap observed in heavily doped p-type GaAs is mainly *indirect*: transitions occur from the Fermi level in the valence band to the bottom of the conduction band. Similar conclusion has been reached by Pankove.[54] Nonparabolicity of the light-hole band, neglected in Fig. 17, would improve the agreement between theory and experiment for p-type GaAs.

AlSb

The electroreflectance spectrum of AlSb has been reported elsewhere.[59] For the sake of completeness we reproduce it in Fig. 18. Due to the reactivity of AlSb with water, the measurements were performed in methyl

[59] M. Cardona, F. H. Pollak, and K. L. Shaklee, Phys. Rev. Letters **16**, 644 (1966).

alcohol. These measurements have provided accurate values of the direct gap E_0 (2.219±0.01 eV at room temperature) which is difficult to observe in conventional optical measurements due to the existence of an indirect gap at 1.6 eV. The $E_0+\Delta_0$ gap (~3 eV according to the spin-orbit splitting data[60]) is hidden under a satellite of the E_1 peak. Two components are seen for each of the E_1 and $E_1+\Delta_1$ peaks. Because of the analogies with GaAs, and since the corresponding reflection peaks[14,61] are quite close to $E_1(1)$ and $E_1+\Delta_1$, we believe that the (1) components are closer to the actual gaps while the (2) components are satellite structure. E_0', $E_0'+\Delta_0'$, E_2, and $E_2+\delta$ peaks are also seen in Fig. 18.

GaP

Figure 19 displays the electroreflectance spectrum of GaP. There is some question as to whether the peak labeled $E_0+\Delta_0$ is the spin-orbit split component of E_0

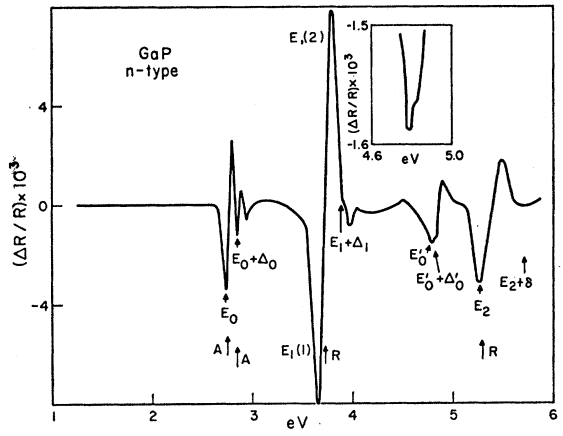

FIG. 19. Electroreflectance spectrum of n-type GaP. $V_{dc}=1.5$ V, $V_{ac}=1$ V rms.

or only a satellite oscillation. Measurements of the GaAs–GaP alloys[56] have shown that this peak is indeed $E_0+\Delta_0$ since it can be followed continuously throughout the whole composition range from the corresponding peak of GaAs. Also, the energy of the E_0, $E_0+\Delta_0$ peaks agrees well with transmission data.[62] The E_1 structure shows also two peaks $E_1(1)$ and $E_1(2)$. No clear indication of the spin-orbit splitting Δ_1 is seen although we have tentatively labeled the shoulder at 3.92 eV $E_1+\Delta_1$ [presumably the (2) component]: Δ_1 is too small (~0.1 eV) to be resolved. E_0' and $E_0'+\Delta_0'$ are barely resolved. E_2 and $E_2+\delta$ are also observed.

GaSb

Figure 20 shows the electroreflectance spectrum of GaSb. The direct edge E_0 is not accessible because of

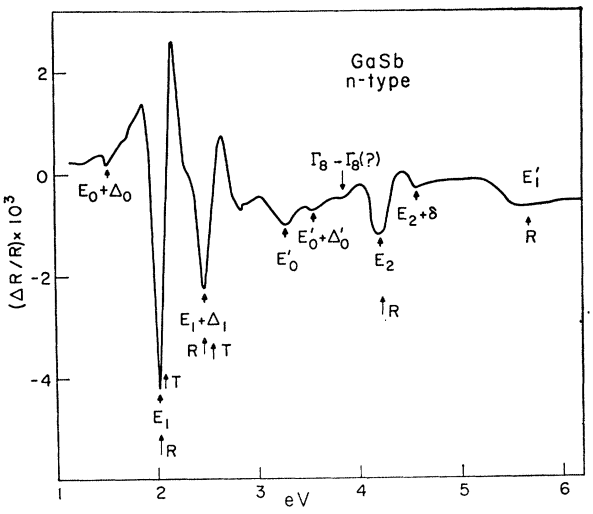

FIG. 20. Electroreflectance spectrum of n-type GaSb. $V_{dc}=1.5$ V, $V_{ac}=1$ V rms.

the infrared cutoff of water. However, the spin-orbit split component $E_0+\Delta_0$ is seen at 1.52 eV. Taking for the direct gap at room temperature[63] 0.72 eV we obtain $\Delta_0=0.80$ eV in very good agreement with the threshold for intra-valence-band transitions[64] in p-type GaSb. The interpretation of the E_1, $E_1+\Delta_1$ peaks does not present the ambiguities of GaAs and GaP: only one prominent peak is seen at E_1 and $E_1+\Delta_1$. The small swings in the opposite direction are clearly satellite structure. The structure between 3 and 4 eV is very similar to that observed in gray tin (see Fig. 12) between 2 and 3.5 eV. Two peaks are seen at 3.27 and 3.56 eV and identified as E_0' and $E_0'+\Delta_0'$, and a weak shoulder at 3.85 eV which seems analogous to the 3.2 eV shoulder of gray tin. The identification of the E_2 and $E_2+\delta$ peaks present no difficulties. Some indication of the unresolved E_1' structure is seen around 5.6 eV.

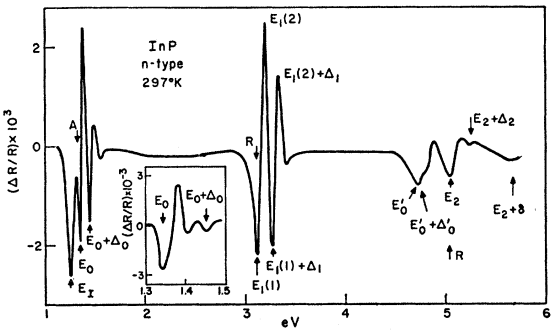

FIG. 21. Electroreflectance spectrum of n-type InP. $V_{dc}=1.5$ V, $V_{ac}=2.5$ V rms. Data in insert were taken at 230°K.

[60] R. Braunstein, Bull. Am. Phys. Soc. 4, 133 (1959).
[61] T. E. Fischer, Phys. Rev. **139**, A1228 (1965).
[62] W. K. Subashiev and S. A. Abagyan, in *Proceeding of the 7th International Conference on the Physics of Semiconductors, Paris, 1964* (Dunod Cie, Paris, 1964), p. 225.
[63] O. Madelung, *Physics of III–V Compounds* (John Wiley & Sons, Inc., New York, 1964), p. 58.
[64] B. B. Kosicki and W. Paul, Bull. Am. Phys. Soc. **11**, 52 (1966).

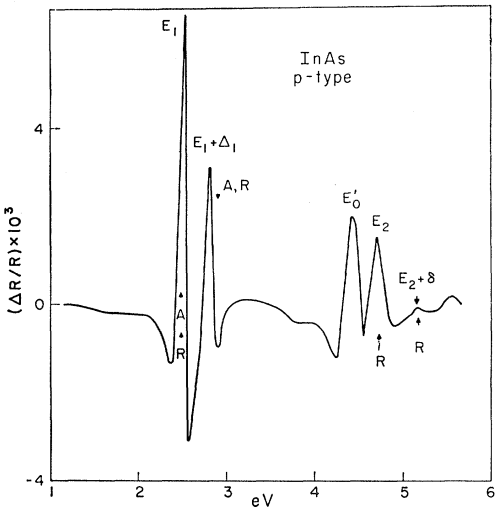

FIG. 22. Electroreflectance spectrum of p-type InAs. $V_{dc}=1.5$ V, $V_{ac}=1$ V rms.

InP

The electroreflectance spectrum of InP is shown in Fig. 21. The complete spectrum was measured at room temperature. A comparison of the fundamental edge structure with absorption data[65] suggests that the first peak at 1.25 eV is due to an impurity level. The direct edge E_0 occurs at 1.34 eV at room temperature, in agreement with absorption data.[65] By analogy with GaP (see Fig. 19) one may label the 1.45 eV peak $E_0+\Delta_0$; this would however imply that the Δ_0 splitting is smaller than Δ_1. While deviations from the $\frac{2}{3}$ rule, discussed in Sec. VII, have been observed, Δ_0 is, for all other materials measured, larger than Δ_1. The peak labeled $E_0+\Delta_0$ could actually be a satellite of E_0. Measurements as a function of field, doping, and temperature (see Fig. 21) seem to indicate however that $E_0+\Delta_0$ is quite insensitive to these parameters and hence corresponds to an actual gap. The insert in Fig. 21 corroborates this assertion: at 230°K the $E_0+\Delta_0$ peak appears well resolved and does not seem to be a satellite since it is stronger than the preceding swing. While these arguments seem convincing, we feel that measurements on InP–InAs alloys are necessary to settle this question.

The $E_1-E_1+\Delta_1$ structure, not resolved in the reflection spectrum at room temperature, is well resolved in Fig. 21. Each peak has two components (1) and (2) of opposite signs; the $E_1(1)$ component is closer to the reflection peak as was the case in GaAs, AlSb, and GaP. The value of Δ_1 derived from Fig. 21 (0.15 ± 0.005 eV) agrees well with estimates from the low-temperature reflection spectrum.[66] The Δ_0' splitting of E_0' is also resolved in Fig. 21.

[65] W. J. Turner, W. E. Reese, and G. D. Pettit, Phys. Rev. **136**, A1451 (1964).
[66] M. Cardona, J. Appl. Phys. **32**, 958 (1961).

The E_2 peak of InP is seen in Fig. 21 at 5.04 eV and $E_2+\delta$ at 5.6 eV. The structure at 5.24 eV has been labeled $E_2+\Delta_2$ for reasons which will be discussed in Sec. VII.

InAs

Figure 22 shows the electroreflectance spectrum of InAs at room temperature. The E_0, $E_0+\Delta_0$ structure falls beyond the low-energy cutoff of water. The E_1, $E_1+\Delta_1$ peaks exhibit only one swing and their interpretation is unambiguous. An estimate of Δ_0' (it should be roughly the average of the value for InP (0.07 eV) and InSb (0.34 eV), i.e., 0.20 eV) indicates that $E_0'+\Delta_0'$ is hidden under the stronger E_2 peak. The peak above E_2 and $E_2+\delta$ ($\sim$5.55 eV) has not been identified.

InSb

The electroreflectance spectrum of InSb is shown in Fig. 23. The E_1, $E_1+\Delta_1$ peaks have only one main component each. The Δ_0' splitting of E_0' is well resolved and a shoulder is seen at 3.7 eV similar to the 3.2 eV shoulder of gray tin (Fig. 12) and that of GaSb at 3.85 eV (Fig. 20). The $E_2-E_2+\delta$ appears well resolved and an indication of E_1' is also apparent. It is noteworthy that the Δ_1 splitting (0.50 eV) is smaller than that found from reflection measurements (0.58 eV). We feel, however, that since considerable discrepancies exist between the various values of Δ_1 reported in the literature[57,67,68] for InSb, electroreflectance measurements as a function of doping, field, and temperature are necessary to settle this question.

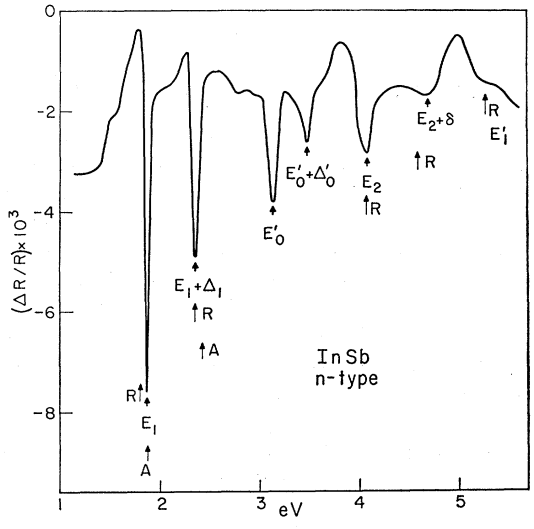

FIG. 23. Electroreflectance spectrum of n-type InSb. $V_{dc}=1.5$ V, $V_{ac}=0.7$ V rms.

[67] J. Tauc and A. Abraham, in *Proceedings of the Conference on the Physics of Semiconductors, Prague, 1960* (Czechoslovak Academy of Sciences, Prague, 1961), p. 375.
[68] F. Lukeš and E. Schmidt, in *Proceedings of the Conference on the Physics of Semiconductors, Exeter, 1962* (The Institute of Physics and The Physical Society, London, 1962), p. 389.

C. Zincblende-Type II–VI Compounds

ZnTe

The spectrum of Fig. 24 is similar to that of Group IV elements and III–V compounds. The direct edge E_0 is now well separated from its spin-orbit split component $E_0+\Delta_0$. The value obtained for Δ_0 ($\Delta_0=0.925$ eV) agrees with that obtained from the reflection spectrum (0.9 eV) and from intra-valence band transitions[69] (0.98 eV). Two swings (1) and (2) appear at E_1 and $E_1+\Delta_1$. The situation is similar to that in GaP, GaAs, InP, and AlSb. Because of the proximity of the (1) swings to the A and R peaks we believe they are quite close to the actual gap while the (2) swings are more likely to be satellites. The E_0' peak is the only other structure which, for this material, still falls within the photon energy range of our system.

CdTe

Figure 25 shows the electroreflectance spectrum of CdTe. The spin-orbit splitting of the fundamental edge is $\Delta_0=0.91$ eV, in agreement with reflection[15] ($\Delta_0=0.9$ eV) and polarimetry[70] data ($\Delta_0=0.9$ eV). The $E_1-E_1+\Delta_1$ structure is considerably different from that reported so far: The leading peaks E_1 and $E_1+\Delta_1$ have opposite sign (phase) to that of germanium, the III–V compounds, and ZnTe. The E_0' peak has again the conventional sign. No other structure appears within the photon energy range of our system.

CdS

Figure 26 shows the fundamental edge of cubic CdS as observed in the electroreflectance spectrum.

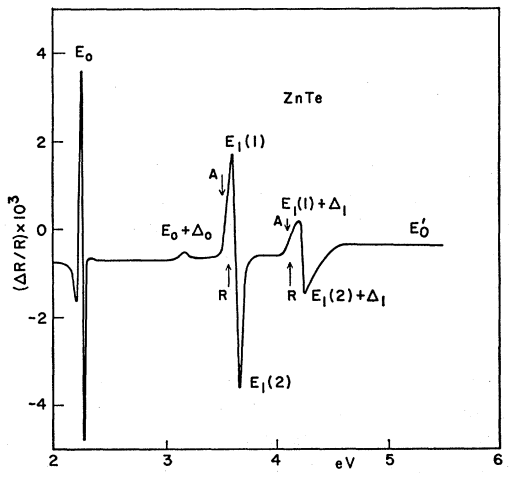

FIG. 24. Electroreflectance spectrum of p-type ZnTe. $V_{dc}=1.5$ V, $V_{ac}=2.5$ V rms.

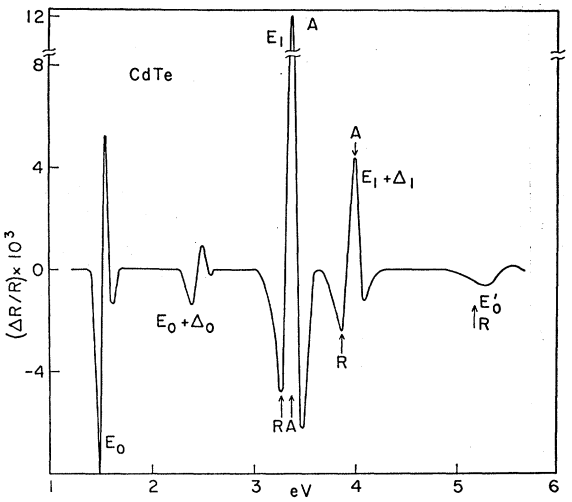

FIG. 25. Electroreflectance spectrum of n-type CdTe. $V_{dc}=1$ V, $V_{ac}=2$ V rms.

The sample was obtained by epitaxial evaporation[71] on GaAs. Structure expected to occur[71] around 5 eV was not seen because of the small sensitivity of our equipment in this region near the high-energy cutoff.

HgSe

Figure 27 shows the electroreflectance spectrum of HgSe. While no peak due to the direct fundamental edge is seen (HgSe may actually be a semimetal like HgTe[72]) a steep rise of $\Delta R/R$ is seen below 1.4 eV. An extension of our measurements below the low-energy cutoff (~1.2 eV) would clarify whether this rise is due to free carrier effects or to a direct edge.

The $E_1-E_1+\Delta_1$ structure is similar in its general aspect to that of CdTe. The phase of the dominant peaks (those close to the absorption and reflection peaks) is also the same as in CdTe and opposite that of all other materials reported so far. Structure likely to be similar to the E_0' of other materials is seen at 5.08 eV.

HgTe

The electroreflectance spectrum of HgTe is shown in Fig. 28. The sign of the E_1, $E_1+\Delta_1$ peaks is the same as in HgSe and CdTe. What seem to be E_0', E_2, and $E_2+\delta$ peaks, of the same sign as in all other materials reported, is seen at 4.14, 4.79, and 5.24 eV respectively.

D. Wurtzite-Type II–VI Compounds

CdSe

Figure 29 shows the electroreflectance spectrum of CdSe. The two upper spectra were obtained for a

[69] N. Watanabe and S. Usui, J. Appl. Phys. (Japan) 4, 467 (1965).
[70] D. T. F. Marple and H. Ehrenreich, Phys. Rev. Letters 8, 87 (1962).
[71] M. Cardona, M. Weinstein, and G. Wolf, Phys. Rev. **140**, A633 (1965).
[72] R. N. Brown and S. Groves, Bull. Am. Phys. Soc. **11**, 206 (1966).

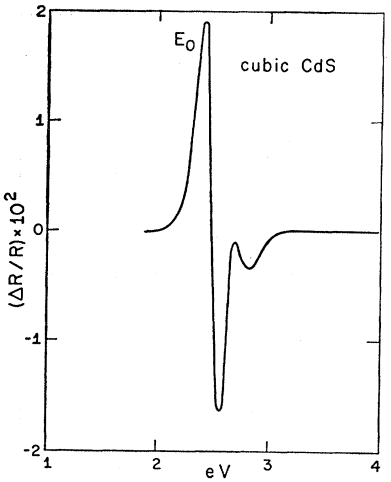

FIG. 26. Electroreflectance spectrum of "cubic" CdS epitaxially deposited on GaAs. $V_{dc}=0.5$ V, $V_{ac}=0.4$ V rms.

cleaved surface containing the hexagonal (c) axis. Measurements were made with polarized light (an air-gap Glan prism was used as a polarizer) for **E** perpendicular and parallel to the c axis. The lower spectrum in Fig. 29 was obtained for a polished and etched surface perpendicular to the c axis (see Table I).

All spectra in Fig. 29 show the direct gap E_0 and its spin-orbit splitting $E_0+\Delta_0$. The E_0 peak occurs 0.029 $\pm$0.005 eV lower in energy for $\mathbf{E}\perp c$ than for $\mathbf{E}\|c$. This fact can be understood in terms of the well-known selection rules for the fundamental absorption edge[73] of wurtzite at $\mathbf{k}=0$. For $\mathbf{E}\perp c$ the top valence band of zincblende, split by the hexagonal crystal field in wurtzite, gives rise to two components in the optical structure: $E_0(A)$ and $E_0(B)$. $E_0(A)$ is only allowed for $\mathbf{E}\|c$. $E_0(B)$ is allowed for both directions of polarization, but it is 3 times stronger for $\mathbf{E}\perp c$ than for $\mathbf{E}\|c$. The A and B lines are not resolved for $\mathbf{E}\perp c$ and hence the peak seen for this polarization is largely due to the A transitions. The crystal field splitting (A-B separation) is 0.029$\pm$0.005 eV, in agreement with exciton measurements at low temperatures (0.025$\pm$0.003 eV, see Ref. 73). The A-C separation, equal to the spin-orbit splitting plus one-half of the crystal-field splitting, is 0.415$\pm$0.005 eV, also in agreement with low-temperature exciton measurements[73] (0.420$\pm$0.004 eV). As discussed in Sec. VII, the $E_1(A_1)$ and $E_1(A_2)$ lines are similar to the E_1, $E_1+\Delta_1$ lines of zincblende. Owing to a selection rule[74] they are only allowed for $\mathbf{E}\perp c$. Similar lines are also observed in the reflection spectrum.[74] The Δ_1 spin-orbit splitting is 0.26 eV. It is interesting to note that the A_1-A_2 lines are relatively stronger (compared to the E_0 lines) for a surface containing c and $\mathbf{E}\perp c$ than for a surface perpendicular to c. This result implies larger reduced effective mass of the corresponding band extrema along the c axis than perpendicular to it. $E_1(B)$ structure[74] allowed for $\mathbf{E}\|c$ and $\mathbf{E}\perp c$, is seen around 5.1 eV.

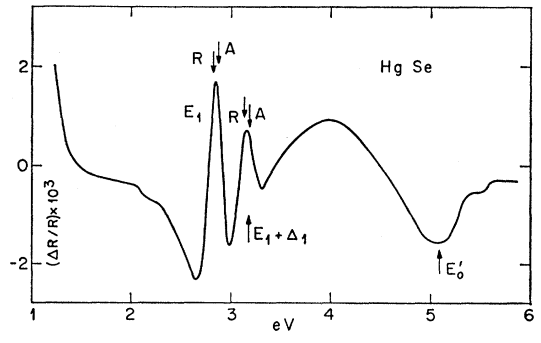

FIG. 27. Electroreflectance spectrum of n-type HgSe. $V_{dc}=1.5$ V, $V_{ac}=1.5$ V rms.

[73] See, for instance, J. O. Dimmock and R. G. Wheeler, Phys. Rev. **125**, 1805 (1962).

CdS

Figure 30 shows the electroreflectance spectrum of CdS in the neighborhood of the fundamental edge. Structure at higher energies has not been seen within the range of our system. The selection rule discussed for CdSe is also apparent. The A-B splitting is 0.014 $\pm$0.003 eV and the A-C splitting 0.073$\pm$0.003 eV, as compared with 0.016 and 0.078 eV obtained from low temperature exciton measurements.[75]

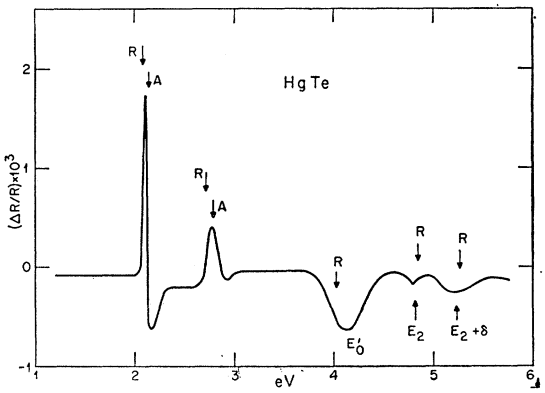

FIG. 28. Electroreflectance spectrum of n-type HgTe. $V_{dc}=1.5$ V, $V_{ac}=0.5$ V rms.

ZnO

The fundamental direct edge of ZnO and its exciton spectrum has been the object of considerable controversy.[76] The lines observed at low temperature and their selection rules cannot be explained with the quasi-cubic model of the wurtzite edge. The spectrum of

[74] M. Cardona and G. Harbeke, Phys. Rev. **137**, A1467 (1965).
[75] D. G. Thomas and J. J. Hopfield, Phys. Rev. **116**, 573 (1959).
[76] Y. S. Park, C. W. Litton, T. C. Collins, and D. C. Reynolds, Phys. Rev. **143**, 512 (1966).

TABLE IV. Energies (in eV) of the peaks observed in the electroreflectance spectra of all germanium and zinc-blende-type materials measured. All data listed were taken at room temperature with the exception of gray tin which was measured at −78°C.

	E_0	$E_0+\Delta_0$	$E_1(1)$	$E_1(2)$	$E_1(1)+\Delta_1$	$E_1(2)+\Delta_1$	E_0'	$E_0'+\Delta_0'$	E_2	$E_2+\delta$	E_1'
Si	4.06	4.13					3.32		4.31		
	±0.1	±0.1					3.38		4.49		
Ge	0.789[a]	1.09[a]	2.12		2.34		3.13	3.32	4.42		
α-Sn			1.36		1.84		2.28	2.63	3.72		4.11, 4.39
											4.89
AlSb	2.22	~3	2.81	2.88	3.21	3.30	3.72	3.99	4.25	4.6	
GaP	2.74	2.84	3.66	3.80			4.78	4.83	5.27	5.74	
GaAs	1.43	1.77	2.89	2.96	3.12	3.19	4.44	4.63	4.99	5.33	
GaSb		1.52	2.03		2.49		3.27	3.56	4.20	4.57	5.50
InP	1.34	1.45	3.12	3.19	3.27	3.34	4.72	4.79	5.04	5.6	
									5.24		
InAs			2.50		2.78		4.44		4.70	5.18	
InSb			1.88		2.38		3.16	3.49	4.08	4.66	5.25
CdTe	1.49	2.41	3.28	3.38	3.87	3.99	5.30				
ZnTe	2.25	3.18	3.61	3.67	4.18	4.27	5.40				
CdS	2.42										
HgSe			2.85		3.15		5.08				
HgTe			2.12		2.78		4.14		4.79	5.24	

[a] See Ref. 4.

Fig. 31 is quite different from that of CdS and CdSe. A number of oscillations, reminiscent of Franz-Keldysh oscillations are seen for both $\mathbf{E}\|c$ and $\mathbf{E}\perp c$; the peaks for $\mathbf{E}\perp c$ all occur 0.037±0.003 eV higher than for $\mathbf{E}\|c$. No structure has been observed at higher energies in the electroreflectance of this material.

A summary of the peaks observed in the electroreflectance spectra of germanium and zinc-blende-type materials is given in Table IV. Table V lists the peaks of wurtzite-type materials.

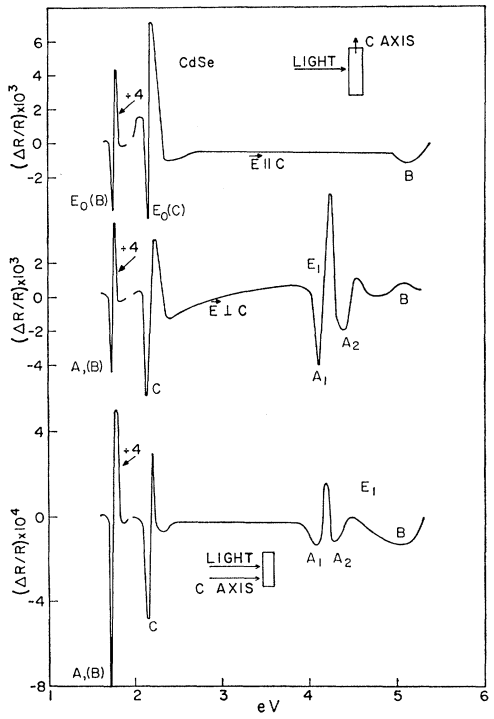

FIG. 29. Electroreflectance spectrum of CdSe (*n*-type). $V_{dc}=1.5$ V, $V_{ac}=1.2$ V rms.

TABLE V. Energies (in eV) of the peaks observed in the electroreflectance spectra of ZnO, CdS, and CdSe. All data listed were taken at room temperature.

	E_0			A		B
	A	B	C	A_1	A_2	
ZnO	3.306	3.340				
CdS	2.452	2.466	2.525			
CdSe	1.717	1.746	2.146	4.11	4.37	5.1

VI. KRAMERS-KRONIG ANALYSIS

As discussed in Sec. III, one must assume an "average" uniform electric field at the surface in order to treat the normal incidence reflection R with Fresnel's equation

$$e^{i\Theta}R^{1/2}=\frac{(n-n_L)+ik}{(n+n_L)+ik}, \tag{8}$$

(Θ is the change in phase under reflection, n and k are the real and imaginary parts of the refractive index of the semiconductor, and n_L the refractive index of the nonabsorbing liquid). Changes in ϵ_1 and ϵ_2 produced by a modulation of the surface field can be calculated from the electroreflectance spectrum in a manner similar to that used in analyzing conventional reflectivity spectra.[45,77] The changes $\Delta\epsilon_1$ and $\Delta\epsilon_2$ are obtained from

[77] M. Cardona and D. L. Greenaway, Phys. Rev. 133, A1685 (1964). The validity of the conventional dispersion relation for the reflectivity [Eq. (9)], when the refractive index of the electrolyte is larger than 1, is not obvious. For a discussion see M. Cardona, lecture given at the NATO Summer Institute on Optical Properties of Solids, Freiburg, 1966 (to be published).

the expressions:

$$\Delta\epsilon_1=\frac{n}{2n_L}(n^2-n_L^2-3k^2)\frac{\Delta R}{R}+\frac{k}{n_L}(3n^2-n_L^2-k^2)\Delta\Theta,$$
$$\Delta\epsilon_2=\frac{k}{2n_L}(3n^2-n_L^2-k^2)\frac{\Delta R}{R}+\frac{n}{n_L}(3k^2+n_L^2-n^2)\Delta\Theta, \quad (9)$$
$$\Delta\Theta(E_0)=\frac{E_0}{\pi}\int_0^\infty \frac{\left(\frac{\Delta R}{R}-\frac{\Delta R_0}{R_0}\right)dE}{E^2-E_0^2}.$$

This calculation requires the knowledge of n and k obtained, in general, from the Kramers-Kronig analysis of conventional reflection data.[45,78] The integration is carried out on an IBM-360 computer using a 5-point integration formula and a mesh of 0.01 eV. It is assumed that no structure occurs below the lower and above the upper energy cutoff of our system. Since most of the structure is symmetric about the $\Delta R/R=0$ axis, and damped by the energy denominator, we feel that this is a reasonable approximation. The index of refraction of water was assumed to be wavelength-independent and equal to 1.33.

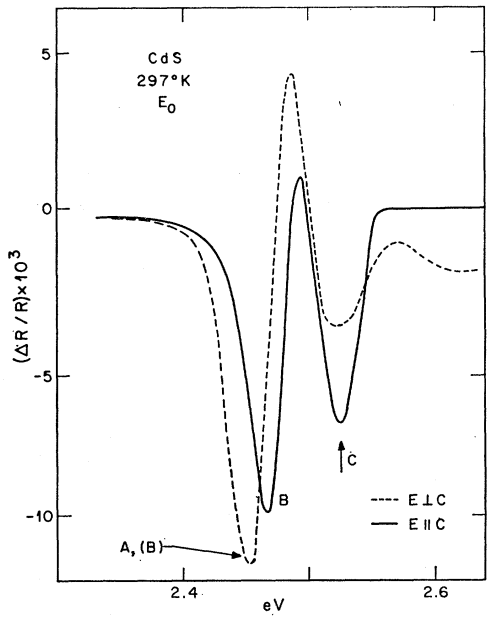

FIG. 30. Electroreflectance spectrum of hexagonal CdS (n-type). $V_{dc}=2$ V, $V_{ac}=2.5$ V rms.

[78] M. Cardona, J. Appl. Phys. **36**, 2181 (1965). We are grateful to Dr. H. R. Phillipp for supplying tabulations of the data in Ref. 45.

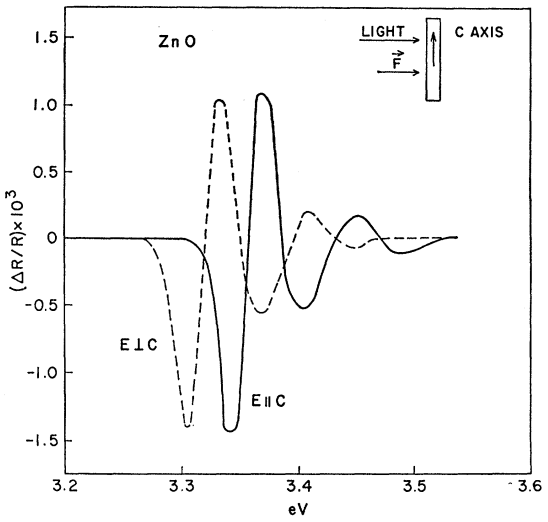

FIG. 31. Electroreflectance spectrum of ZnO. $V_{dc}=0$ V, $V_{ac}=0.02$ V rms.

Figure 32 shows $\Delta\epsilon_1$ and $\Delta\epsilon_2$ obtained from the spectrum in Fig. 8 for germanium. We note that the E_1, $E_1+\Delta_1$ peaks are similar in sign and general shape to those calculated for M_0 singularities. This seems to be in disagreement with the M_1 nature generally accepted for these singularities[79]: The effect of a longitudinal field (along [111] on a [111] M_1 critical point) on $\Delta\epsilon_1$ would be the mirror image with respect to a vertical line through the gap E_1 of that in Fig. 32. A transverse field at the M_1 edge (perpendicular to [111]) should produce an effect qualitatively similar to that at an M_0 edge. We find, however, that the M_0 line shapes[31] resemble more closely the curves of Fig. 32. Because of the partial superposition of the two spin-orbit split lines no great value should be attached to this conclusion: the singularity responsible for E_1 and $E_1+\Delta_1$ is most likely of M_1 type as indicated by band calculations.[11,12] It is noteworthy that the splitting of the E_1, $E_1+\Delta_1$ peaks is 0.20 eV in Fig. 32. This value agrees

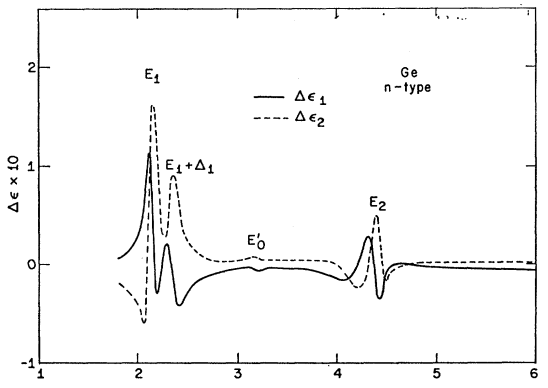

FIG. 32. $\Delta\epsilon_1$ and $\Delta\epsilon_2$ as obtained from the Kramers-Kronig analysis of the data of Fig. 8.

[79] J. C. Phillips, Phys. Rev. **146**, 584 (1966).

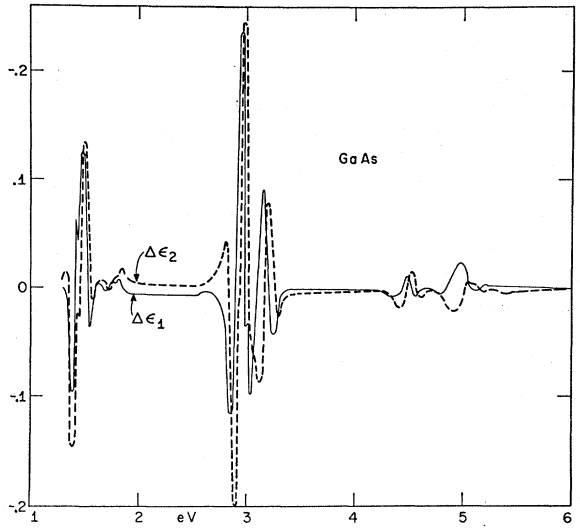

FIG. 33. $\Delta\epsilon_1$ and $\Delta\epsilon_2$ as obtained from the Kramers-Kronig analysis of the data of Fig. 14.

better with the results of the reflection spectrum[14] than that obtained from Fig. 8 (0.22 eV). Line-shape effects due to the close proximity of E_1 and $E_1+\Delta_1$ are undoubtedly responsible for this discrepancy.

The E_0' structure of Fig. 32 is too weak for a detailed discussion. The E_2 peaks clearly correspond to an M_1 singularity with a longitudinal field: oscillations (one swing between 4.2 and 4.3 eV) are seen *below* the 4.43-eV gap.

Figure 33 shows the results of the Kramers-Kronig analysis of the data of Fig. 14. The $E_1-E_1+\Delta_1$ peaks are now clearly of the M_1-transverse field variety. This is best illustrated in Fig. 34, where an attempt has been made to fit $\Delta\epsilon_1$ and $\Delta\epsilon_2$ at E_1 to the theoretical $F(\eta)$ and $G(\zeta)$ curves[31] for an M_1-transverse field critical point. We believe that the modulation is large enough so as to yield for $\Delta\epsilon$ the functions F and G rather than their derivatives (see Sec. III). The fit of the experimental curves is better than for any other critical point configuration and it would presumably improve if broadening effects were taken into account. The energy gap required for the fit is 2.88 eV, quite close to

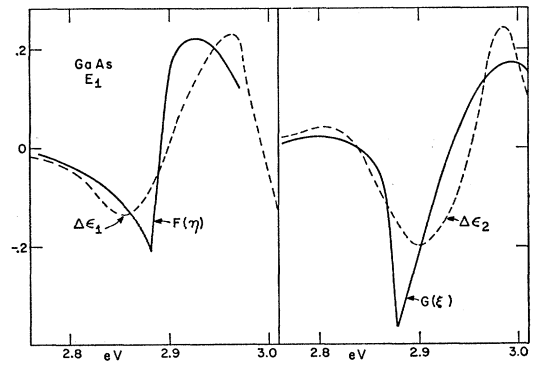

FIG. 34. $\Delta\epsilon_1$ and $\Delta\epsilon_2$ around the E_1 peaks of Fig. 33 (dashed lines) and fit with the theoretical expressions of Ref. 31 (full line).

the energy of the $E_1(1)$ electroreflectance peak (2.89 eV). This constitutes further proof that $E_1(1)$ corresponds to a gap while $E_1(2)$ is a satellite peak.

Figures 35 and 36 show the results of the Kramers-Kronig analysis of the $\mathbf{E}\|[001]$ curves of a [110] silicon surface (Figs. 10 and 11, respectively). The E_2 peaks of Fig. 35 are similar to these of germanium (Fig. 32) while those of Fig. 36 are quite different. Figures 35 and 36 seem to indicate a change in the nature of the critical points when reversing the dc bias. We think, however, that any such conclusions would be premature at the present time.

Figure 37 shows the results of the Kramers-Kronig analysis of the CdTe data (Fig. 25). The E_0 and $E_0+\Delta_0$ edges can be explained as the Franz-Keldysh effect of M_0 edges. The E_1, $E_1+\Delta_1$, and E_0' peaks are similar in shape to those of GaAs (Fig. 33).

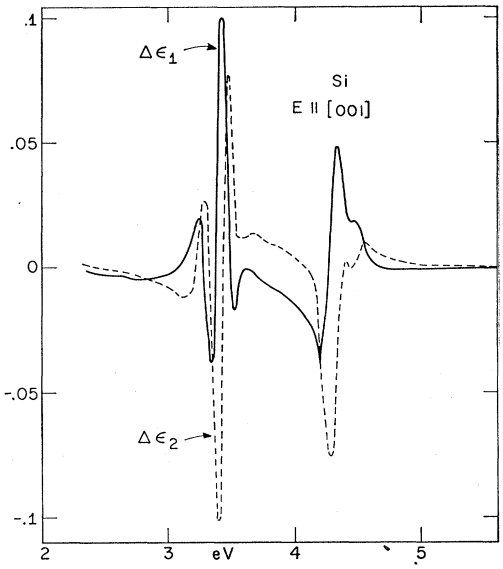

FIG. 35. $\Delta\epsilon_1$ and $\Delta\epsilon_2$ for a [110] silicon surface with the electric field of the light along [001] and a *positive* dc bias, as obtained from the data of Fig. 10.

We have done the Kramers-Kronig analysis of the electroreflectance spectra of Sec. V for all materials for which optical constants are available. The $\Delta\epsilon_1$ and $\Delta\epsilon_2$ spectra obtained are in general similar to those discussed above. For the sake of brevity, the remaining $\Delta\epsilon_1$ and $\Delta\epsilon_2$ spectra are not presented in this paper.

VII. DISCUSSION

A. Group-IV Elements

The electroreflectance spectra discussed in Sec. V supply a great deal of information about spin-orbit splittings. The Δ_0 splitting of germanium is 0.29 eV, as obtained by Seraphin and Hess.[4] The semimetal character of gray tin, involving the reversal of the $\Gamma_{25'}$ and $\Gamma_{2'}$ bands[21] (see Fig. 2) prevents us from seeing the $E_0+\Delta_0$ peak and thus determining Δ_0 (the $\Gamma_7^+-\Gamma_8^+$

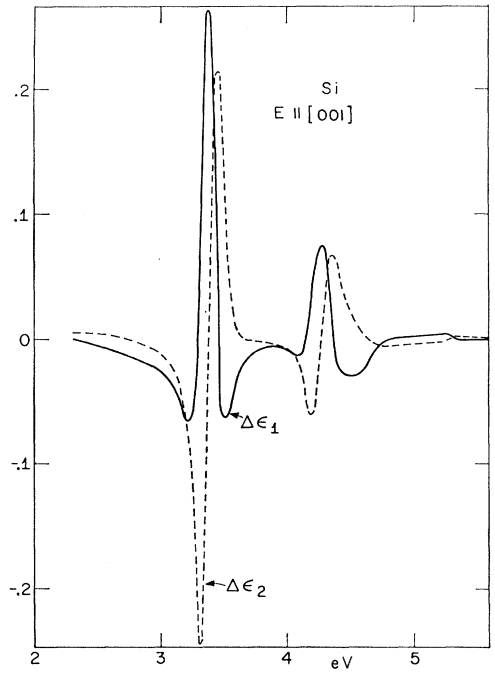

FIG. 36. $\Delta\epsilon_1$ and $\Delta\epsilon_2$ for a [110] silicon surface with the electric field of the light along [001] and a negative dc bias, as obtained from the data of Fig. 11.

transitions between the split-off band and the lowest conduction band are forbidden and hence probably too weak to be seen in electroreflectance). The splitting observed for the E_0' peak of silicon (0.06 eV) is close to the Δ_0 splitting.[80] We cannot, however, explain the selection rule of Fig. 10 on the basis of this assumption. We feel therefore that an interpretation of the E_0' splitting of silicon has to be postponed until the various transitions contributing to this peak are sorted out. The Δ_0 splitting of gray tin can be estimated from the observed Δ_1 splitting (0.48 eV) by the two-thirds rule mentioned earlier: the spin-orbit splitting of $\Gamma_{25'}(\Delta_0)$ should be three-halves of the Λ_3 splitting (Δ_1). This rule is only valid if the nonzero matrix elements of the spin-orbit Hamiltonian are the same at $\Gamma_{25'}$ as at Λ_3. While not strictly true, this remains a good approximation for group IV elements and for zincblende-type materials with constituents of the same row of the periodic table.[9,12] A more accurate scheme has been suggested[12] to relate the Δ_0 splitting of group IV materials to Δ_1 and to the splitting of the Γ_{15} conduction band (Δ_{15}). In the whole-zone $\mathbf{k}\cdot\mathbf{p}$ representation of the band structure of group IV materials,[12] the uppermost valence band along the [111] direction can be written as a linear combination of *four* $\mathbf{k}=0$ states. Of these four, only two ($\Gamma_{25'}$ and Γ_{15} of Fig. 2) contribute to the spin-orbit splitting. In the [100] direction, the uppermost valence band is a linear combination of three $\mathbf{k}=0$ states. Also, only two of them contribute to the spin-orbit interaction since the third one is mainly d like. The spin-orbit splitting along [100] and [111] is therefore only a function of two parameters: Δ_0 and the splitting of the Γ_{15} conduction band (Δ_{15}). Symmetry requires that the splitting at X_4 be zero; this imposes a relationship between Δ_{15} and Δ_0 and leaves us with only one independent spin-orbit splitting parameter. All spin-orbit splittings can be calculated provided one is known experimentally. The linear combination of $\mathbf{k}=0$ states giving the valence-band wave functions is roughly the same for all Group IV materials (for a given $\mathbf{k}$). At the X_4 point the condition of zero splitting becomes, using the linear combinations of Ref. 12,

$$0.54\Delta_0-0.43\Delta_{15}=0. \tag{10}$$

The coefficients in Eq. (10) are good to $\pm 8\%$ for all Group IV elements. Table VI shows the splittings Δ_{15} for silicon and germanium calculated from the experimental values of Δ_0 with Eq. (10). For gray tin Δ_0 is not known experimentally. Its value has been calculated from the experimental value of Δ_1 (0.48 eV) using Eq. (10) and the relationship

$$\Delta_1=\tfrac{2}{3}[0.94\Delta_0+0.12\Delta_{15}], \tag{11}$$

valid for α-Sn and Ge to $\pm 2\%$.

The spin-orbit splitting at the $L_{3'}$ valence-band point and at the lowest L_3 conduction band, can be calculated with the expressions

$$\Delta(L_{3'})=\tfrac{2}{3}[0.66\Delta_0+0.14\Delta_{15}]$$
and
$$\Delta(L_3)=\tfrac{2}{3}\times 0.43\Delta_{15}. \tag{12}$$

It has been suggested in Sec. II that the E_0' transitions occur at a point in the [100] direction near $\mathbf{k}=0$. Critical points occur, or nearly occur, in this region in Figs. 2 and 3 for transitions between the 2 top valence bands and the second lowest conduction band. These transitions should have a splitting Δ_0' smaller than Δ_1

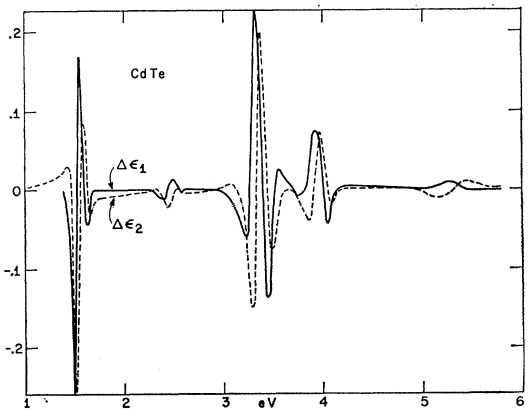

FIG. 37. $\Delta\epsilon_1$ and $\Delta\epsilon_2$ as obtained from the Kramers-Kronig analysis of the data of Fig. 25.

[80] S. Zwerdling, K. J. Button, B. Lax, and L. M. Roth, Phys. Rev. Letters 4, 173 (1960).

TABLE VI. Calculated and experimental values (in eV) of several spin-orbit splittings in germanium-like materials. The experimental numbers in boldface have been used for the determination of one adjustable parameter required for the calculations.

	Δ_0		Δ_1		Δ_{15}	Δ_0'		$\Delta(L_{3'})$	$\Delta(L_3)$
	calc.	expt.	calc.	expt.	calc.	calc.	expt.	calc.	calc.
Si	0.044	**0.044**[a]	...	...	0.055	0.025		0.024	0.016
Ge	0.29[b]	**0.29**	0.19	0.20[c]	0.36	0.17	0.19	0.16	0.10
α-Sn	0.77	...	0.48	**0.48**	0.97	0.39	0.35	0.43	0.28

[a] See Ref. 80.
[b] See Ref. 4.
[c] From Fig. 32.

since along the [100] direction the spin-orbit splittings of the $\Gamma_{25'}$ and Γ_{15} components of the wave function subtract.[12] The maximum spin-orbit splitting in the [100] direction is given approximately by

$$\Delta_0' = \tfrac{2}{3}[0.93\Delta_0 - 0.06\Delta_{15}]. \quad (13)$$

The critical points occur near the region of maximum splitting. The values of Δ_0' calculated with Eq. (13) for germanium and gray tin agree reasonably well with those observed experimentally.

Since the energy separation between E_0' and the 3.3 eV shoulder of gray tin is 1 eV, very close to the Δ_{15} splitting, we have speculated[50] that the 3.3 eV shoulder is due to $\Gamma_{25'}(\Gamma_8^+) \rightarrow \Gamma_{15}(\Gamma_8^-)$ transitions. The peaks seen in Fig. 12 at 4.11, 4.39, and 4.89 eV seem to correspond to $L_{3'} \rightarrow L_3$ transitions. Structure due to these transitions should occur, according to calculations[50] at 4.08, 4.34, 4.48, and 4.73 eV (a quadruplet because of the spin-orbit splittings of $L_{3'}$ and L_3).

The E_2 peak of silicon (see Figs. 10 and 11) has two components with a separation of 0.2 eV. These two components are likely to be the M_1 and M_2 singularities required to produce the strong peak observed in the reflection spectrum. Comparison with band calculations[19] suggests that the lower energy singularity occurs very near X while the higher energy occurs in the [110] (Σ) direction. It is noteworthy that these two singularities are not resolved in the germanium and gray tin spectra.

It has been shown in Fig. 9 that the E_1 peak becomes quite weak (with respect to $E_1+\Delta_1$) in heavily doped p-type germanium ($P=8\times10^{19}$ cm^{-3}). A possible explanation of this effect may be the emptying of the valence band states which contribute to E_1 as acceptors are added. A decrease in E_1 would be expected when the Fermi level reaches the region where E_1 transitions originate. Such an effect would obviously not affect the $E_1+\Delta_1$ structure until much higher dopings (not attainable in practice). The Fermi level for $P=8\times10^{19}$ is roughly 0.2 eV below the top of the valence band. The Λ singularity occurs for valence band states approximately 0.35 eV below $\Gamma_{25'}$ and therefore this explanation is not quantitatively correct.

B. III–V Compounds

In the spirit of the $\mathbf{k}\cdot\mathbf{p}$ approach described in Sec. VIIa, the band structure of a III–V compound is obtained by adding an antisymmetric potential to the potential of the isoelectronic Group IV element. The antisymmetric potential mixes the $\Gamma_{25'}$ and Γ_{15} states of the Group IV material and hence the spin-orbit splittings of the Γ_{15} valence and conduction bands become a linear combination of the Δ_0 and Δ_{15} of the corresponding Group IV material. The antisymmetric potential adds an antisymmetric term to the spin-orbit splitting. This term introduces a new matrix element Δ^- to our calculation: it is the matrix element of the antisymmetric spin-orbit interaction between Γ_{15} and $\Gamma_{25'}$.

Since the coefficients of the linear combination of $\Gamma_{25'}$ and Γ_{15} which form the Γ_{15} valence and conduction band wave functions do not vary much from one compound to the other, we can represent the spin-orbit splitting of the Γ_{15} conduction (Δ_{15}) and valence (Δ_0) bands as

$$\begin{aligned}\Delta_0 &= 0.83\tilde{\Delta}_0 + 0.17\tilde{\Delta}_{15} + 0.75\Delta^-,\\ \Delta_{15} &= 0.17\tilde{\Delta}_0 + 0.81\tilde{\Delta}_{15} - 0.75\Delta^-,\end{aligned} \quad (14)$$

where $\tilde{\Delta}_0$ and $\tilde{\Delta}_{15}$ are the spin-orbit splittings of the corresponding isoelectronic Group IV material. In the case of constituent atoms of different rows of the periodic table, we take for $\tilde{\Delta}_0$ and $\tilde{\Delta}_{15}$ the average of the Group IV materials of the same row as the III–V atoms. The coefficients in Eqs. (14) are those calculated[81] for GaAs. Equations (14) enable us to determine Δ^- if Δ_0 is known. These values are listed in Table VII together with the values of Δ_{15} calculated from Δ^- and the second of Eqs. (14).

The spin-orbit splitting Δ_1 of the E_1 peaks can also be approximately obtained for all III–V compounds from the orbital wave functions of GaAs:

$$\Delta_1 = \tfrac{2}{3}[0.77\tilde{\Delta}_0 + 0.20\tilde{\Delta}_{15} + 0.61\Delta^-]. \quad (15)$$

The results of this calculation are presented in Table VII. Deviations from the two-thirds rule appear automatically in Eqs. (14) and (15) when the constituent atoms do not belong to the same row of the periodic table and hence Δ_0 is very different from $\tilde{\Delta}_0$ and $\tilde{\Delta}_{15}$. As a result Δ^- is very large and the two-thirds rule does not hold due to the different contribution of Δ^- to Eqs. (14) and (15). Deviations from the two-thirds rule observed for GaSb, AlSb, and GaP are well

[81] F. H. Pollak, C. W. Higginbotham, and M. Cardona, J. Phys. Soc. Japan Suppl. 21, 20 (1966).

TABLE VII. Calculated and experimental values (in eV) of several spin-orbit splittings in zinc-blende-like materials. The experimental numbers in boldface have been used for the determination of one adjustable parameter required for the calculations.

	Δ_0		Δ_1		Δ^-	Δ_0'		Δ_{15}	Δ_2		$\Delta(L_{3'})$	$\Delta(L_3)$
	expt.	calc.	expt.	calc.	calc.	expt.	calc.	calc.	expt.	calc.	calc.	calc.
AlSb	**0.75**[a]	0.75	0.40	0.45	0.44	0.27	0.47	0.10		0.28	0.34	0.087
GaP	**0.10**	0.10	~0.1	0.095	−0.047	0.05	0.072	0.17		0.007	0.087	0.075
GaAs	**0.34**	0.34	0.23	0.22	0.051	0.19	0.17	0.26		0.073	0.18	0.11
GaSb	**0.80**	0.80	0.46	0.49	0.33	0.29	0.48	0.31		0.29	0.39	0.16
InP	**0.11**	0.11	0.15	0.11	−0.42	0.07	0.086	0.74	0.20	0.21	0.14	0.24
InAs	**0.43**[b]	0.43	0.28	0.29	−0.16	···	0.22	0.67		0.030	0.28	0.25
InSb	**0.82**[c]	0.82	0.50	0.53	0.026	0.33	0.45	0.78		0.091	0.50	0.33

[a] See Ref. 60.
[b] F. Matossi and F. Stern, Phys. Rev. **111**, 472 (1958).
[c] M. Cardona, K. L. Shaklee, and F. H. Pollak. Phys. Letters **23**, 37 (1966).

explained with this method. The deviation observed for InP is too large to be fully accounted for by this method.

A similar argument yields for Δ_0' along [100]:

$$\Delta_0'=\tfrac{2}{3}[0.75(\tilde{\Delta}_0)^2+0.70(\tilde{\Delta})^2+1.35\Delta_0\Delta^-]^{1/2}. \quad (16)$$

The values of Δ_0' obtained from Eq. (16) are also tabulated in Table VII together with those determined from the electroreflectance spectra. Agreement with experiment is good for materials with small Δ_0'. For materials with large Δ_0' Eq. (16) is a bad approximation since the spin-orbit coupling to the lower (Γ_7) valence band has been neglected. The agreement is improved by a detailed calculation taking this interaction into specific account and using the wave functions of the material. As an example, for AlSb we calculate[81] $\Delta_0'=0.27$ eV.

The fourfold X_4 degeneracy of germanium is split in zinc-blende-type materials due to the lack of inversion symmetry. The method used above yields for this splitting (Δ_2) in the III–V compounds,

$$\Delta_2=\tfrac{2}{3}[0.1\tilde{\Delta}_0+0.09\tilde{\Delta}_{15}+0.96\Delta^-]. \quad (17)$$

The results of Eq. (17) are also in Table VII. Notice that for InP $\Delta_2=0.21$ eV. The splitting between E_2 and the peak labeled $E_2+\Delta_2$ (for obvious reasons), is 0.20 eV. This assignment is, however, only tentative and requires further experimental evidence.

Table VII also lists the spin-orbit splittings at the L_3' valence band point and the L_3 conduction band [$\Delta(L_{3'})$ and $\Delta(L_3)$], calculated with the expressions:

$$\begin{aligned}\Delta(L_{3'})&=0.5892\tilde{\Delta}_0+0.2370\Delta^-\\ \Delta(L_3)&=0.4027\Delta_0-0.1750\Delta^-\end{aligned} \quad (18)$$

obtained from the $\mathbf{k}\cdot\mathbf{p}$ orbital wave functions of GaAs.

C. II–VI Compounds

The method of calculating spin-orbit splittings described above cannot be easily extended to the II–VI compounds. In the first place, the Λ singularity seems to occur very near the edge of the zone[82] (L) and some difficulties have been encountered in extending the $\mathbf{k}\cdot\mathbf{p}$ approach to the II–VI compounds, especially at the edge of the zone.[83] Also, the decomposition of the crystal potential of a II–VI compound into a symmetric and an antisymmetric part may not yield as the symmetric part the potential of the isoelectronic Group IV material. We have tried, without success, to fit the Δ_0 and Δ_1 splittings of CdTe and ZnTe by using only one adjustable parameter (Δ^-) and the wave functions obtained from a preliminary $\mathbf{k}\cdot\mathbf{p}$ calculation for ZnSe. We would obviously be able to fit the two experimental splittings by using also $\tilde{\Delta}_0$ as an adjustable parameter, but we doubt the value of such a calculation. A less sophisticated approach of calculating the Δ_0 spin-orbit splittings from spectroscopic atomic data has been proposed.[14,17] The two-thirds rule holds well for CdTe and ZnTe but considerable deviations exist for CdSe and ZnSe.[10]

ACKNOWLEDGMENTS

The samples used in these experiments were obtained through the courtesy of Dr. T. E. Fischer, Dr. V. Giriat, Dr. S. Groves, Dr. D. L. Greenaway, Dr. E. Hockins, Dr. J. J. Loferski, Dr. M. I. Nathan, Dr. W. Paul, Dr. D. C. Reynolds, and Dr. C. R. Whitsett. We would also like to acknowledge the assistance of R. L. Ludin in the performance of the experiments and C. W. Higginbotham in the programming of the Kramers-Kronig analysis.

[82] M. L. Cohen and T. K. Bergstresser, Phys. Rev. **141**, 789 (1966).
[83] Due to the strong admixture of upper states produced by the antisymmetric potential, in the II–VI compounds the bands calculated by $\mathbf{k}\cdot\mathbf{p}$ do not reach the edge of the zone with zero slope.